

This is to certify that the thesis entitled

MEASUREMENTS OF CYCLE-TO-CYCLE VARIABILITY OF FUEL INJECTORS

presented by

Joshua C. Bedford

has been accepted towards fulfillment of the requirements for the

Masters of Science degree in Mechanical Engineering

Major Professor's Signature

7/20/04

Date

MSU is an Affirmative Action/Equal Opportunity Institution

LIBRARY Michigan State University

PLACE IN RETURN BOX to remove this checkout from your record.

TO AVOID FINES return on or before date due.

MAY BE RECALLED with earlier due date if requested.

DATE DUE	DATE DUE	DATE DUE

6/01 c:/CIRC/DateDue.p65-p.15

MEASUREMENTS OF CYCLE-TO-CYCLE VARIABILITY OF FUEL INJECTORS

Ву

Joshua C. Bedford

A THESIS

Submitted to
Michigan State University
in partial fulfillment of the requirements
for the degree of

MASTER OF SCIENCE

Department of Mechanical Engineering

2004

cycle var

T

emission

Engine

variabil

nitroger

velocit

injecto

6μs, de

this pr

fluid n

injecte

deviat

ABSTRACT

MEASUREMENTS OF CYCLE-TO-CYCLE VARIABILITY OF FUEL INJECTORS

By

Joshua C. Bedford

The goal of this project was to develop a technique for measuring the cycle-to-cycle variability of fuel injectors. This method can then be used to improve injector design. More consistent and precise fuel injectors have the potential to improve emissions, fuel efficiency, and engine performance.

The experiments for this study were conducted at the Michigan State University Engine Research Laboratory on a test setup specifically designed to evaluate the variability of fuel injectors. The setup consists of a vessel pressurized by compressed nitrogen, a Dantec laser Doppler anemometry (LDA) system that measures the centerline velocity of fuel through a quartz tube, and a Cosworth IC 5460, which controls the injector. The detector on the LDA system is capable of resolving Doppler bursts at up to 6µs, depending on the level of seeding, thus giving a detailed time/velocity profile. From this profile, the mass injected in each injection event was calculated using appropriate fluid mechanics equations. These calculated values were compared with cycle-averaged measurements to validate the accuracy of this technique. Finally, profiles of the mass injected per cycle have been generated and the variability calculated in terms of standard deviation, coefficient of variation, etc.

Ian his continu would like assistance a Sasak for members h Yuan Shen

research. Schock for

the unstead

Stuecken

experiment

engines fro

I'd like to

prayers. su

where I am

ACKNOWLEDGMENTS

I am truly grateful to the people who have helped me through my schooling and research. I would like to extend my sincere thanks and appreciation to Dr. Harold Schock for giving me the opportunity to work at the Engine Research Laboratory, and for his continual guidance and support. Thanks to Dr. Giles Brereton for his assistance with the unsteady flow calculations and to Dr. Farhad Jaberi for being on my committee. I would like to thank Ed Timm for teaching me how to use the LDA system, Tom Stuecken for his creative input and for fabricating the mounts required for the experimental setup, and Andy Fedewa for help at the lab. I genuinely appreciate the assistance and friendship they have provided throughout my time here. I also thank Andy Sasak for his help in writing the calculation program. Thanks to all the remaining members here at the lab including Jan Chappell, Mulyanto Poorte for his editing skills, Yuan Shen, and Boon-Keat Chui. Thanks to Jack Tennis for encouraging my interest in engines from a young age and continually answering my automotive questions. Finally, I'd like to thank my entire family, particularly my parents Jon and Angie, for your prayers, support, and encouragement throughout the years. I would have never made it to where I am today without you.

List of Table

List of Figu

List of Sym

CHAPTER

Introduction

1.1

1.

CHAPTI Experime

CHAP Experi

TABLE OF CONTENTS

List of Tab	les	vi
List of Figu	ıres	vii
List of Sym	nbols and Abbreviations	ix
CHAPTER	.1	
Introductio	n	1
1.1	Motivation	1
1.2	Fuel Injection History	2
1.3	Gasoline Port Fuel Injector Design	3
1.4	Previous Work	
1.5	Calculating the Mass Flow Rate	11
CHAPTER	. 2	
Experimen	tal Equipment	14
2.1	Dantec Fiber LDA Measurement System	14
2.2	Injectors	16
2.3	Injector Control System	
2.4	Fuel Delivery System	17
2.5	Mounting Hardware and Alignment	18
2.6	Oscilloscope	
2.7	Seed and Dispersal Devices	
2.8	Mass Balance	20
2.9	Delay Box	
2.10	·	
2.1	1 Software	21
CHAPTER	3.3	
Experimen	tal Procedure	23
3.1		
3.2	LDA Technique	
3.3	•	

CHAPTER Results and 4.1

4.2

CHAPTER Conclusions

CHAPTER Recommend

APPENDIC

App Deta

App Calc

App Evo

REFEREN(

Results and	Discussion	
4.1	Results	
	4.1.1 Injector #1 Results	
	4.1.2 Injector #2 Results	
4.2	Discussion	• • • •
	4.2.1 Comparison of Injectors #1 and #2	
	4.2.2 Sources of Variability	
	4.2.2.1 Cosworth Variability	
	4.2.2.2 Sources of Error	
CHAPTER	5	
Conclusion	s	••••
Conclusion CHAPTER	s	
Conclusion CHAPTER Recommen APPENDIC	s6 dations	••••
Conclusion CHAPTER Recomment APPENDIC App	6 dations CES pendix A	
Conclusion CHAPTER Recomment APPENDIC App	s6 dations	
Conclusion CHAPTER Recomment APPENDIC App Deta	6 dations CES pendix A	
Conclusion CHAPTER Recomment APPENDIC App Deta App	s	
Conclusion CHAPTER Recomment APPENDIC App Deta App Calc	6 dations CES Dendix A ails of the Mass Flow Equation Dendix B	

Table 1: Pot

Table 2: Fu

Table 3: Inj

Table 4: Co

Table 5: Pr

Table 6: Re

LIST OF TABLES

Table 1: Potential gains for individual cylinder fuel control	7
Table 2: Fuel/Air ratio range	39
Table 3: Injection control system variability statistics	40
Table 4: Comparison between mass balance and LDA measurements	43
Table 5: Probe volume variables	54
Table 6: Results of probe volume calculations	55

Images in this thesis are presented in color.

Figure 1: The

Figure 2: Fu

Figure 3: Ism

Figure 4: Ism

Figure 5: Pre

Figure 6: Thi

Figure 7: Sch

Figure 8: Res

Figure 9: Gra

Figure 10: D

Figure 11: D

Figure 12: Fu

Figure 13: Co

Figure 14: Fu

Figure 15: M

Figure 16: Ho

Figure 17: A

Figure 18: St.

Figure 19: Ex

Figure 20: Ph

Figure 21: Li

LIST OF FIGURES

Figure 1: The Rochester fuel injection system for the '57 Corvette	2
Figure 2: Fuel injector diagram	4
Figure 3: Ismailov's test setup	6
Figure 4: Ismailov's velocity and mass flow rate profiles	6
Figure 5: Presence Probability Image (PPI) for a set of 30 injections	9
Figure 6: Three different spray patterns overlaid on the PPI	9
Figure 7: Schematic of ambient test performed by Delphi for determining concentration and droplet sizing	10
Figure 8: Results of measuring concentration and droplet sizing	10
Figure 9: Graph of the unsteadiness of a fuel injection event	12
Figure 10: Dantec ion laser	14
Figure 11: Dantec transmitting (top) and receiving	15
Figure 12: Fuel injectors used	16
Figure 13: Cosworth injector control module	17
Figure 14: Fuel delivery system	18
Figure 15: Mounting setup	19
Figure 16: Hewlett-Packard Infinium oscilloscope	19
Figure 17: AND GX-4000 mass balance	20
Figure 18: Stanford Research Systems delay box	21
Figure 19: Experimental setup	23
Figure 20: Photograph of experimental setup	25
Figure 21: LDA schematic (shown in back-scatter configuration)	26

Figure 22: Cy

Figure 23: Th

Figure 24: M

Figure 25: C

Figure 26: Th

Figure 27: M

Figure 28: A

Figure 29: PI

Figure 30: PI

Figure 31: V

Figure 32: V

Figure 33: Pr

Figure 34: P

Figure 35: B

Figure 36: A

Figure 37: V

Figure 38: V

Figure 39: Bu

Figure 40: V

Figure 41: V

Figure 42: V.

Figure 43: Cur

Figure 22:	Cycle-averaged centerline velocity plot with injector voltage	3 1
Figure 23:	Three consecutive cycles from Injector #1	32
Figure 24:	Mass injected chart for Injector #1	3
Figure 25:	Cycle averaged centerline velocity plot with injector voltage	34
Figure 26:	Three consecutive cycles from Injector #2	35
Figure 27:	Mass injected chart for Injector #2	16
Figure 28:	Average centerline velocities along with applied voltage	17
Figure 29:	PDF of mass injected for Injector #1	8
Figure 30:	PDF of mass injected by Injector #2	8
Figure 31:	Voltage plot of the injection control system	Ю
Figure 32:	Velocity plots for Injector #1 with and without air	ŀ5
Figure 33:	Probe volume diagram and intensity distribution	52
Figure 34:	Probe volume dimensions	53
Figure 35:	Beam refraction sketch and values	;4
Figure 36:	Average plot of early experiments	6
Figure 37:	Velocity profiles for a 15-inch copper fuel delivery line	8
Figure 38:	Velocity profiles for a 20-inch rubber fuel delivery line	;8
Figure 39:	Bubble sizes used to seed the flow	;9
Figure 40:	Velocity profiles taken through time with seed and water	50
Figure 41:	Velocity profiles taken through time with water and bubbles	51
Figure 42:	Velocity plots for Injector #1 with and without air	53
Figure 43:	Cut-away of Injector #2	54

Symbol

Α Avg c CCD cm CO dB E deg D_L DI ECU F h HC HCCI Hg Hz i ICFC IMEP kHz LDA m mg mm ms mV MHz mW N2 NOx OC PDA Pdf PPI Psi R ROSA

SAE

LIST OF SYMBOLS AND ABBREVIATIONS

<u>Symbol</u> <u>Description</u>

A cross-sectional area

Avg average c wave speed

CCD charged-coupled device

cm centimeter CO carbon dioxide

dB decibel

E elastic modulus, expander ratio

deg degree

DLdiameter of laserDIdirect injectionECUengine control unitFfocal Lengthhwall thicknessHChydrocarbons

HCCI homogeneous charge compression ignition

Hg mercury
Hz hertz
i incidence

ICFC individual cylinder fuel control IMEP indicated mean effective pressure

kHz kilohertz

LDA laser Doppler anemometry

mass flow rate m milligrams mg millimeters mm milliseconds ms mV millivolts MHz megahertz mW megawatts N_2 nitrogen **NOx** nitrous oxides

OC optical concentration
PDA particle dynamics analyzer
Pdf probability density function
PPI presence probability image
psi pounds per square inch

R radius

ROSA rapidly operating electromagnetic secondary

actuator

SAE Society of Automotive Engineers

SOI start of injection

μm υ $\begin{array}{cccc} t & & & & & \\ s & & & & & \\ u & & & & \\ velocity \\ \overline{u} & & & & \\ u_{cl} & & & & \\ weighting velocity \\ W(t) & & & & \\ V_{ellipse} & & & \\ \end{array}$

δ incremental value λ wavelength 3.14159 π θ angle density ρ non-dimensional time τ micrometer μm kinematic viscosity υ

engines, v

A

measured to test inj

and will a

potential

control ov

1.2 Fu

its develop

pressure. an

inputs to thi

CHAPTER 1

INTRODUCTION

1.1 Motivation

As engineers strive to improve the performance of modern internal combustion engines, well-designed engine control systems and their components become of greater importance. The more accurately the engine control system measures air flow and meters fuel flow, the more control engineers have over the output of the engine. This project focuses on measuring the cycle-to-cycle variability of a fuel injector and its control system. If a stable injection control system is developed, and there is no variation in the output voltage, current, and duration, the variation of the fuel injector alone can then be measured. The technique developed during this study will allow injector manufacturers to test injectors thoroughly, viewing real-time performance on an individual cycle basis, and will assist in improving injector designs. Improved injection consistency has the potential to reduce cycle-to-cycle variability in combustion quality, thus improving control over fuel economy and emissions.

1.2 Fuel Injection History

Fuel injection technology has made great advances since Robert Bosch pioneered its development in the 1920's. Bosch originally developed fuel injectors for use in diesel engines. These early fuel injection systems were entirely mechanical, in that timing, pressure, and droplet distribution were all controlled by mechanical means. The only inputs to this early control system were throttle position and engine speed. During World

War II, Bosch developed a fuel injection system for German airplanes. The injectors were spring-loaded open full-time and oscillated rapidly to maximize atomization. With such crude parts and primitive controls, early fuel injection systems were essentially "controlled leaks" [1].

After the war, most aircraft industries did not continue fuel injection research, but instead concentrated their efforts on the development of turbine engines. Automotive manufacturers were content to make minor developments to the inexpensive carburetor, so advances in fuel injection were temporarily on hold [2]. In 1949, a young American hot-rodder named Stuart Hilborn re-ignited interest in this field when he developed a fuel injection system for his race car. Shortly after, Mercedes sold fuel-injected models in the early 1950's, but with little success. Chevrolet worked with carburetor manufacturer Rochester to develop a fuel injection system called the Rochester Ramjet (pictured below

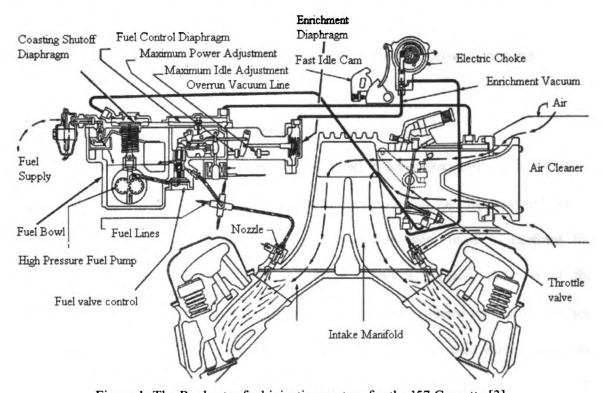


Figure 1: The Rochester fuel injection system for the '57 Corvette [3].

from article by Woron [3]) for the '57 Corvette and the Pontiac Bonneville. Even with these advances, fuel injection was not widely accepted until the 1970's when emissions and fuel economy concerns coincided with advances in electronics technology to make fuel injection more desirable and affordable.

Early systems employed a throttle-body design in which one or two injectors replaced the carburetor to meter fuel. With the development and advancement of microprocessors, multi-port and sequential multi-port fuel injection systems were developed. Currently, all new cars and trucks produced and sold in the U.S. are fuel-injected.

Modern injection systems are highly developed feedback control systems that take into account several parameters, including engine speed, load, throttle position, mass air flow, oxygen concentration in exhaust, coolant temperature, manifold pressure, etc. Fuel injection performance is better today than ever before, but there is clearly room for improvement in the area of cycle-to-cycle variability in the fuel delivery systems.

1.3 Gasoline Port Fuel Injector Design

In order to understand possible sources of fuel injection variability, it is important to have an understanding of the basic components of a typical fuel injector and how it functions. In this study, gasoline port fuel injectors were used to perform the experiments. Figure 2 on the following page shows a cutaway diagram of the components that make up a standard gasoline electronic fuel injector for a port injection configuration. A fuel injector is essentially an electronically controlled valve. When the injector is energized by the engine control unit (ECU), an electromagnet (solenoid)

moves a pluto reveal a injector, the opened [4] combustion and fuel injuittle as a feelight speed.

stroke in 0.2

Ther

pressure of fluctuations

moves a plunger that is connected to the pintle. This plunger only moves about 0.15 mm to reveal a calibrated annular passage. Because a pressurized fuel line supplies the injector, the fuel travels through this passage and sprays out the nozzle when the pintle is opened [4]. The nozzle is designed to atomize the fuel for improved mixing and combustion. When the injector is no longer energized, the return spring closes the pintle and fuel injection ceases. For solenoid-actuated injectors, this entire process may take as little as a few milliseconds for multiple injection systems or for engines running at very high speed. Piezoelectric injectors, on the other hand are capable of completing one stroke in 0.2 ms [5].

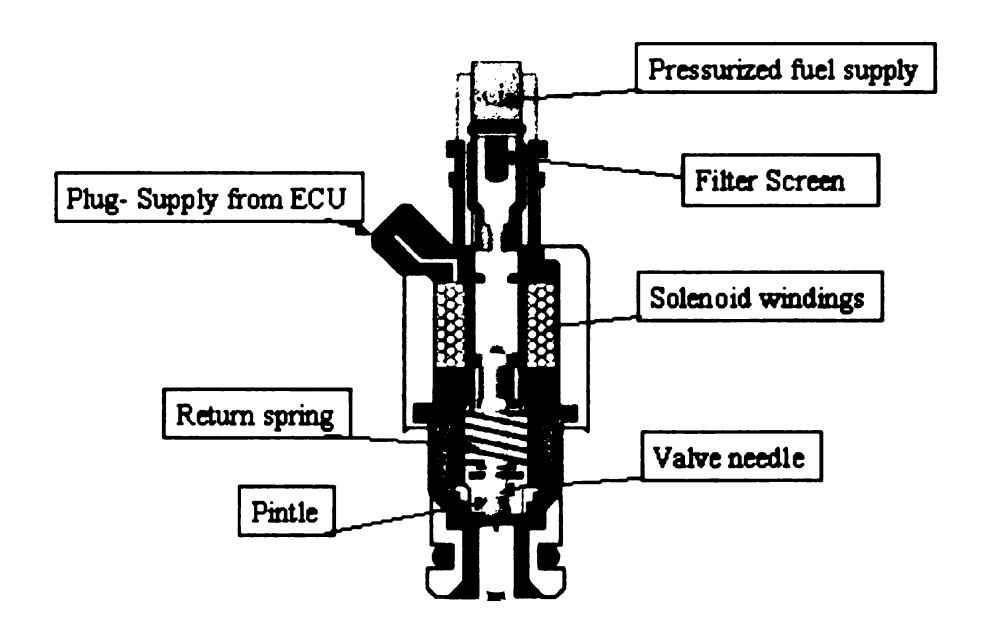


Figure 2: Fuel injector diagram [3].

There are several potential sources of variability in a fuel injection system. The pressure of the fuel supplied should be constant to reduce variability. Pressure fluctuations can be caused by a fuel pump or by pressure waves propagating in the fuel

this proj

Voltage

pulse win

not to re

1.4 F

R

variabilit
complete
Laborato
measuren
research
six injecti
system.
Evaluation

In 1 Generated

Injection 5

attributes 1

system.

lines as a result of injection events [6]. Air in the fuel lines or in the injector itself will cause wild oscillations that contribute to variability, as was discovered over the course of this project. Dirty or partially clogged injectors certainly contribute to variability. Voltage and current supplied to the solenoid must be consistent as they directly control pulse width, or the duration of the injection event. Although the focus of this project is not to redesign fuel injectors, but to measure and quantify variability, it is important to keep these sources of variability in mind.

1.4 Previous Work

Relatively little research has been reported in the area of measuring cycle-to-cycle variability of the total mass injected by fuel injectors. Previous work in this field was completed by Dr. Murad Ismailov at the Michigan State University Engine Research Laboratory in 2003. He studied high-pressure (up to 30,000 psi) diesel injectors using measurement techniques like those discussed in this report. The focus of Ismailov's research was to develop an injector control system that was capable of delivering up to six injections per cycle. Ismailov also calculated the mass injected by this multiple-burst system. His work is published in two SAE papers. In his paper titled "Performance Evaluation of a Multi-Burst Rapidly Operating Secondary Actuator applied to Diesel Injection System" [7], Ismailov mentions that cycle-to-cycle variation is observed. He attributes this largely to the cyclic pressure deviation in the common rail fuel delivery system.

In his next paper, "Quantification of Instantaneous Diesel Flow Rates in Flow Generated By a Stable and Controllable Multiple Injection System (ROSA)" [8],

Ismailov discusses the measurement technique in greater detail and includes centerline velocity plots. A diagram of the setup is shown in Figure 3, and graphs of centerline velocity and mass flow rates are shown in Figure 4.

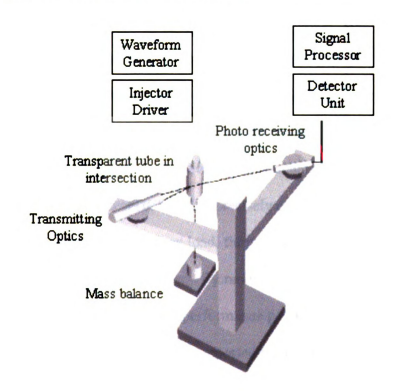


Figure 3: Ismailov's test setup [8].

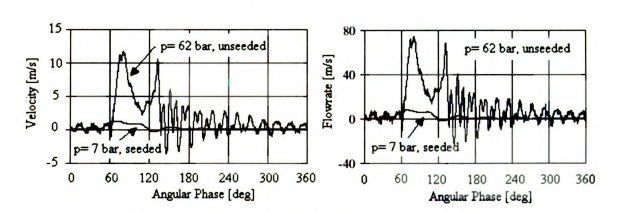


Figure 4: Ismailov's velocity and mass flow rate profiles [8].

From the paper, it is unclear what equations were used to accomplish this, but it is clear that the centerline velocity trace was involved in the calculations. Nevertheless, Ismailov's work was instrumental in that it provided the basis of the experimental procedure used in this study.

While no other published reports were found where velocity was measured before the injector, other papers measured variability in fuel injectors. Delphi Corporation has shown interest in this topic for several years. A 1999 SAE paper written by Kainz and Smith titled "Individual Cylinder Fuel Control with a Switching Oxygen Sensor" [10] discusses controlling the fuel/air ratio by closely monitoring the oxygen content in the exhaust for each cylinder. They also developed an adaptive control algorithm called Individual Cylinder Fuel Control (ICFC) that precisely controls the fuel delivered to each cylinder based on current inputs such as load, throttle position, etc. and also the oxygen sensor history for that particular cylinder. By modeling this control system, Delphi was able to predict several significant engine performance gains. These gains are listed in the table on the next page. The emissions were reported to be lower, more consistent, and

Table 1: Potential gains for individual cylinder fuel control [10].

	НС	со	NOx	Torque	IMEP
Cylinder Imbalances max +/-8% tolerances	6.0	49	70	60	5.6%
Balanced Cylinders	5.5	29	14	61.21 (+2.0%)	2.5%
Emissions (ppm)				Fuel Economy	Driveabili

mo

cyl

ope

inc

im

inj

Im Inj

Tł

an it

сy

pr

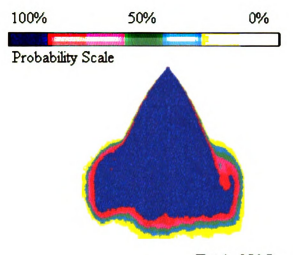
th Co

eŋ

fo

more repeatable. Variability in IMEP was also lowered using this technique. Fuel economy increased because the lean limit was extended. Typically, the leanest-running cylinder determines the lean drivability limit. For an engine with ICFC, each cylinder is operated closer to the lean limit. This resulted in improved idle quality as well as increased torque and improved engine efficiency. While this study did not focus on improving the performance of the fuel injector itself, it shows the benefit of a fuel injection system operating with greater control and precision.

Another interesting study is described in an SAE paper titled "Application of an Imaging-based Diagnostic Technique to Quantify the Fuel Spray Variations in a Direct-Injection Spark-Ignition Engine," written by Hung, Chmiel, and Markle (Delphi) [11]. This paper focuses on capturing the magnitude of pulse-to-pulse variability in penetration and spray geometry. Using a high-resolution grayscale CCD digital camera and triggering it by pulsing a laser, they were able to generate pictures of the spray distribution for each cycle. The images were then post-processed with Optimas^R image analysis software to produce a Presence Probability Image (PPI) like the one shown in Figure 5. Images like this give important insight into how consistently the fuel and air are likely to mix. Consistent mixing is vital if one is concerned with the cycle-to-cycle performance of an engine, particularly for homogenously charged compression ignition (HCCI). The following figures illustrate the results of this research effort.



Total of 30 Images

Figure 5: Presence Probability Image (PPI) for a set of 30 injections [11].

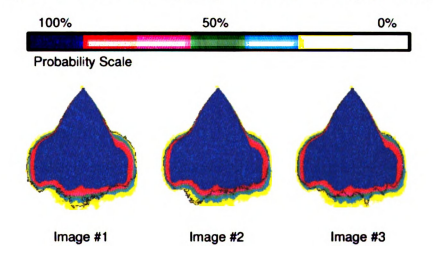


Figure 6: Three different spray patterns (black outline) overlaid on the PPI (color) [11].

There are several publications in the field of droplet sizing of the spray from fuel injectors. Lefebvre discusses several measurement techniques (mechanical, electrical, and optical methods) in his book <u>Atomization and Sprays</u> [12]. Another noteworthy publication is an SAE paper by Hung et al., "A Novel Transient Drop Sizing Technique for Investigating the Role of Gasoline Injector Sprays in Fuel Mixture Preparation" [13]. This method measures the concentration and droplet sizing at various locations from the

injector. The setup and results are shown in the figures that follow. In the second figure, SOI refers to the start of injection.

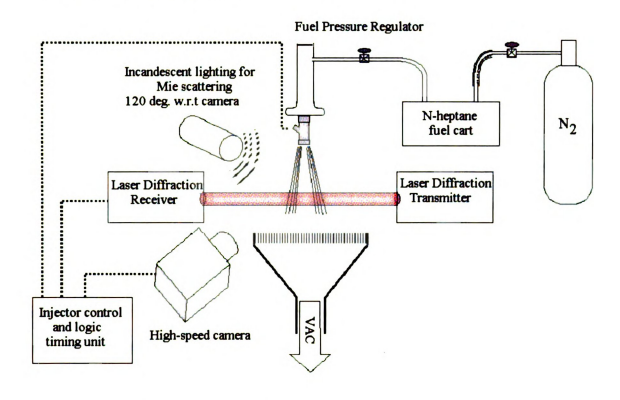


Figure 7: Schematic of ambient test performed by Delphi for determining concentration and droplet sizing. [13]

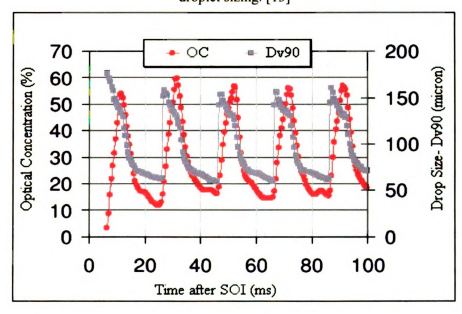


Figure 8: Results of measuring concentration and droplet sizing [13]

These results are interesting because they show a very large range of droplet sizes. The size of the droplet directly affects how quickly the fuel mixes with the air. In port injection, the hot intake valve assists in vaporizing the fuel; but in a direct injection engine, droplet size could have a significant effect on performance and emissions.

1.5 Calculating the Mass Flow Rate

Determining the mass injected per cycle is at the core of this measurement technique. Some of the key parameters available for calculation include fluid density, viscosity, the areas and lengths of the fuel delivery and quartz tubes, and centerline velocity plotted as a function of time. The problem can be viewed as an internal flow in a circular pipe of problem. The mass flow rate was first calculated. This was then plotted as a function of time. From this, the mass injected could be calculated by simply integrating over the correct portion of time. Initially, a plug flow profile was assumed

$$\dot{m} = \rho \cdot u_{cl} \cdot A \tag{1}$$

(Eqn. 1) to simplify calculations. In this equation, ρ is the density, u_{cl} is the centerline velocity, and A is the cross-sectional area of the tube through which the fluid is flowing. Later on, a laminar parabolic velocity profile was assumed (Eqn. 2). The plug flow assumption over-predicted the mass injected

$$\dot{m} = \frac{1}{2} \cdot \rho \cdot u_{cl} \cdot A \tag{2}$$

(based on an average measured value over 50 cycles) by roughly 60% because it did not account for the viscous interaction between the fluid and the wall. The steady state, laminar, parabolic profile assumption under-predicted the mass flow by about 45%. It was reasonable to assume laminar flow because the Reynold's number typically ranged

from 0-2000 with only a very small portion occasionally spiking to 2100. After further analysis, however, it was determined that a local, or quasi-steady assumption was not valid.

Equation (2) is an equation for measuring the level of unsteadiness in a flow [14].

This equation is a ratio of the unsteady to viscous term in the

$$\left| \frac{1}{u} \frac{du}{dt} \cdot \frac{R^2}{v} \right| \ge 1 \tag{3}$$

streamwise momentum equation. A flow is considered to be unsteady for absolute values greater than or equal to 1. Figure 9 is a graph of the unsteadiness of a typical injection event. Clearly this shows a great deal of unsteadiness. Therefore, a laminar unsteady pipe flow solutions must be implemented.

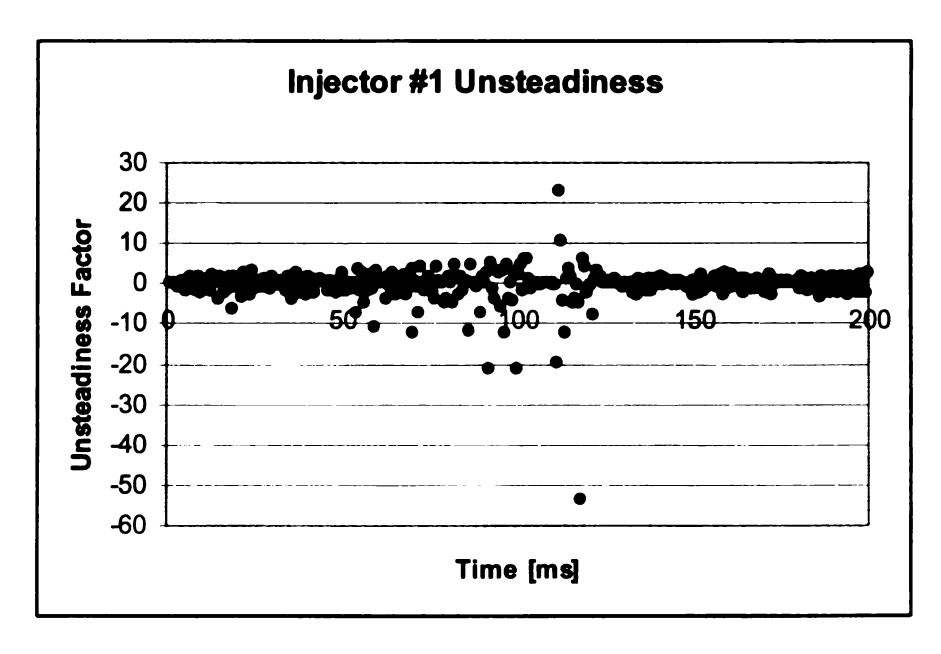


Figure 9: Graph of the unsteadiness of a fuel injection event.

A solution to this highly unsteady flow pipe problem was developed previously by Brereton [14]. This solution is an exact unsteady solution of the laminar NavierStokes equations for arbitrary, unsteady duct flow and essentially consists of a quasisteady solution plus an unsteady correction term. The solution takes into account the flow's "history". The influence of the velocity profile history is weighted by using an inverse convolution integral. The general form of the solution is given below where

$$\dot{m}(t) = \rho \cdot (\pi \cdot R^2) \cdot U(t) \tag{4}$$

and

$$U(t) = \frac{1}{2}u_{cl}(t) + \frac{d}{dt}(u_{cl}(t)) * W(t).$$
 (5)

In Equation (4), the first term is the quasi-steady velocity term and the second term is the unsteady correction term. Also, u_{cl} is the centerline velocity and W(t) is the inverse convolution weighting function. The details for this weighting function are given in Appendix A.

CHAPTER 2

EXPERIMENTAL EQUIPMENT

2.1 Dantec Fiber PDA Measurement System

The Particle Dynamics Analysis (PDA) system was used to measure the centerline velocity profile during each injection event. The Dantec Fiber PDA system consists of the following major components:

· Laser: one 120-mW ion laser



Figure 10: Dantec ion laser [15].

- Transmitting optics: Fiber Flow optical system consists of a beam splitter, Bragg cell, fiber optic cables, and a transmitting probe with a 310 mm focal length
- Receiver: 57X40 Fiber PDA receiving optics



Figure 11: Dantec transmitting (top) and receiving (bottom) [16].

- 58N70 Fiber PDA detector unit
- Signal processor: 58N80 PDA enhanced Particle Dynamics Analyzer
- Computer: for post-processing and storage of data
- · Software: PDA Flow and Particle Software
- Mounting equipment (breadboard, C-clamps, traverses, etc.)

Because the flow was measured in a very small quartz tube, the setup needed to be capable of fine adjustments to ensure that the probe volume is located in the center of the flow. The system was noted to be sensitive to vibrations sent through the floor. For this reason, all other large machines that produce these vibrations were shut off during experimentation.

2.2 Injectors

Two gasoline port fuel injectors were used for analysis. The first was an injector from the 2004 Toyota Prius Hybrid (1.5 liter four-cylinder engine). This injector had 12 tiny holes for increased fuel atomization. The second injector was a port injector made by Siemens (111084) for the 2004 Daimler-Chrysler Hemi 5.7 liter V8 engine. Pictures of these injectors along with close-up views of their nozzles are shown in Figure 12. For



Figure 12: Fuel injectors used (left- Toyota Prius injector, right- Chrysler Hemi injector). the remainder of this report, the Toyota injector will be referred to as Injector #1 and the Chrysler injector as Injector #2.

2.3 Injector Control System

The fuel injector was controlled by the Cosworth IC5460 Engine Control System.

Using the Flowbench interface software, the injector was set to fire every 200 ms with a



Figure 13: Cosworth injector control module.

9 ms duration. In order for the results to be accurate concerning the fuel injector's variability, it is vital that the injector controller introduce as little variability as possible.
In order for this to occur, the frequency and pulse width must be extremely consistent.

2.4 Fuel Delivery System

Compressed nitrogen was used to pressurize the fuel delivery system. This method was chosen over a fuel pump because it provides constant, even pressure. A beaker containing the fuel is placed in a pressure vessel connected to the compressed nitrogen and the fuel injector. The system was then raised to 50 psi. A diagram of the fuel delivery system is shown in Figure 14. The material and length of the fuel delivery tube greatly affected the flow dynamics due to the propagation of pressure waves. Several materials and lengths were tested, and a nylon tube was eventually selected. It was also determined that the presence of air bubbles or air pockets located either in the fuel lines or in the fuel injector itself greatly affects the centerline velocity profile. The details of these tests will be discussed in a later section. The final setup consisted of a nylon fuel delivery tube with a diameter of 6 mm and a length of 60 cm, a quartz tube with a diameter of 2.97 mm and a length of 10.5 cm, a fuel injector, and a drain tube.

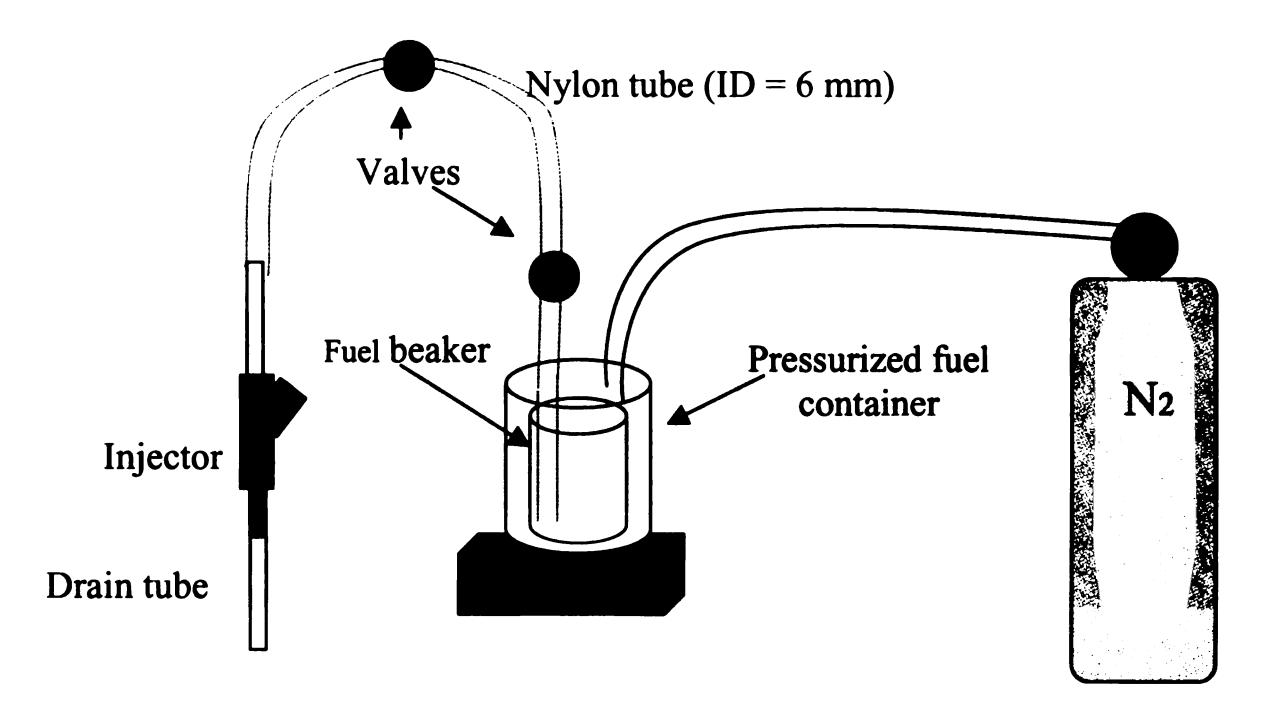


Figure 14: Fuel delivery system.

2.5 Mounting Hardware and Alignment

When designing the test rig for this experiment, an effort was made to insure that the laser transmitting and receiving probes could be positioned precisely. It was also important that these components remain fixed in place. The laser transmitter, receiver, and fuel injector were all mounted on a large breadboard. The injector was mounted on a custom-made bracket that was attached to a Newport optical mounting rod (Model 75). This rod allowed for vertical adjustment. The laser-transmitting probe was mounted on a dual rod system because of its size and weight. This dual rod setup was mounted on an x-y translation stage (Newport Model 400). The laser-transmitting probe had a built-in swivel base that allowed for rotation in the x-y plane. Thus, the probe could be adjusted in the x, y, and z axes and was free to rotate in the x-y plane. The receiving optic was mounted in a similar fashion but used a single optical mounting rod. When these rigs were complete, they were capable of making the fine adjustments necessary to properly

align the optics. As a result, good data rates were achieved. Pictures of the mounting hardware are shown below.



Figure 15: Mounting setup.

2.6 Oscilloscope

The Hewlett-Packard Infinium oscilloscope (Model # 54810 A) was used to monitor Doppler bursts as well as to measure the variability of the Cosworth injector controller. In order to obtain valid results, it was important to get a good strong Doppler signal from the detector. The oscilloscope was particularly useful for making fine



Figure 16: Hewlett-Packard Infinium Oscilloscope.

adjustments in the detector alignment. It was also used to measure the variability in the frequency and voltage output of the Cosworth controller. Statistics such as standard deviation of voltage, frequency, and rise time were recorded.

2.7 Seed and Dispersal Devices

Two types of seed were used in the experiments for this project. Early on, polyamid seeding particles from Dantec were used. These particles have a mean particle diameter of $5 \mu m$ and are recommended for use in fluids with densities similar to water. In order to distribute the seed throughout the working liquid, a Nuova II magnetic stirrer was used. Later, a microbubble seeding technique was developed and implemented. A high-speed blender was used to entrain and distribute these bubbles throughout the liquid.

2.8 Mass Balance

An AND GX-4000 mass balance was used to measure the mass of the fuel injected over a series of 50 injections. The value was then divided to calculate the cycle-averaged mass injected per cycle. This value was compared with the calculated values for validation purposes.



Figure 17: AND GX-4000 mass balance.

2.9 Delay Box

A Stanford Research Systems delay box (Model DG535) was used to center the injection pulse in the time plot. Without the delay box, the injection pulse was located at the endpoints of the graph making it more difficult to analyze.



Figure 18: Stanford Research Systems delay box.

2.10 Vacuum Pump

A Dayton Electric Speedaire vacuum pump (Model 78866) was used to evacuate air from the fuel delivery system as well as from the fuel injector. This pump is capable of pulling up to 23 inches of mercury (in Hg).

2.11 Software

Microsoft Excel and C++ were used extensively for performing analysis and calculations. The program developed in C++ requires a .txt file that is exported from Dantec's PDA Flow and Particle Software. It has inputs for the tube radius, fluid density, kinematic viscosity, and approximate beginning and ending of injection event. For simplicity, the program defaults to the test conditions used in the lab (water at standard atmospheric conditions). The program then sorts the data so that it is arranged in consecutive injections, performs the necessary unsteady, laminar, pipe flow mass

calculations as previously discussed (Appendix A), and outputs the mass injected per cycle along with a sparse value that describes the density of the data over the cycle. This sparse value is important for understanding whether the output is reasonable. If the time resolution of the data is too small, interpolation error becomes a problem. The program also outputs statistics such as average, standard deviation, and coefficient of variation.

CHAPTER 3

EXPERIMENTAL PROCEDURE

3.1 Complete Test Rig Setup and General Procedure

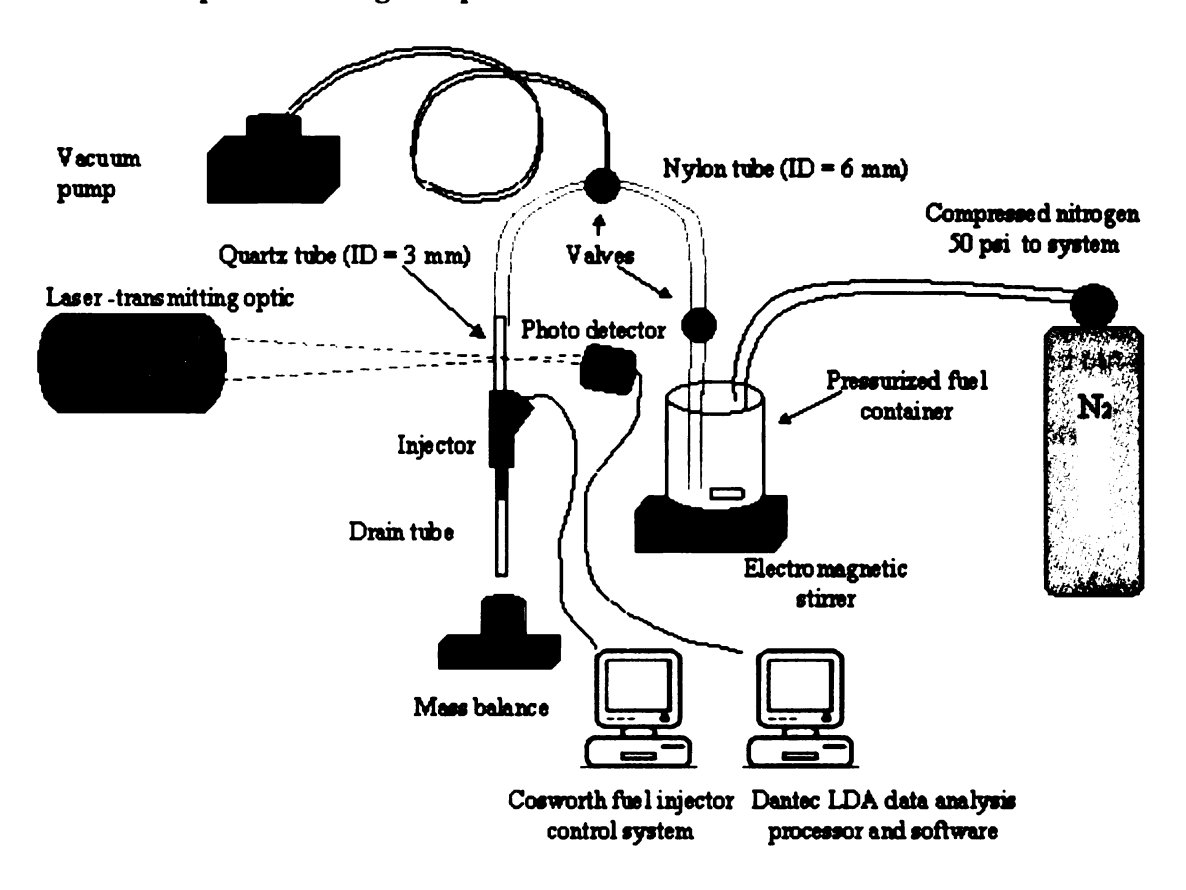


Figure 19: Experimental setup.

General Procedure:

- Attach injector to quartz tube using rubber hose and hose clamps. Fasten the
 drain tube to the nozzle end of the injector. Hook up the wires from the injector
 control unit to the connector.
- 2.) Turn on the Cosworth control system, laser, computers, oscilloscope, and delay box.

- 3.) Load the PDA Flow and Particle software to control the LDA system and load the Flowbench software to control the Cosworth injection control device.
- 4.) Seed the working fluid (water for this case) and fill the beaker located in the pressure vessel. Seal the pressure vessel completely. Any leak will result in a rapid evacuation of the liquid when pressure applied.
- 5.) Connect the pressure vessel to a tank of compressed nitrogen. Slowly bring up the pressure and look for leaks. If no leaks exist, raise the pressure up to 50 psi.
- 6.) Evacuate any air from the fuel lines and injector using the vacuum pump. Make sure the valve to the container vessel is shut off so that only air is pulled out of the fuel supply line and injector and not all of the fluid from the beaker exits.
- 7.) When laser comes on, align the laser transmitter and detector.
- 8.) Fire the injector and observe the Doppler bursts on the oscilloscope. Make fine adjustments to the LDA detector until the bursts are at their maximum.
- 9.) With the injector still running, trigger the PDA system to collect data.
- 10.) If the time resolution is not good enough (Velocity Data Rate less than 2 kHz), adjust the High Voltage and S/N Validation parameters and collect data again.
- 11.) If time resolution is good, collect as much data as is needed, then depressurize system, and power down electronic devices.
- 12.) Post-process data using Excel or C++ program.

This procedure was developed through months of testing. The details of these various tests and some of the important lessons learned can be viewed in Appendix C.



Figure 20: Photograph of experimental setup.

3.2 LDA Technique

Laser Doppler Anemometry (LDA) was chosen to measure the centerline velocity of the fuel entering the fuel injector. , LDA was desirable because of it is non-intrusive, directionally sensitive, and has high spatial and temporal resolution. In general, LDA works by processing data from laser light that is reflected by particles in the flow field (Doppler bursts). Two lasers intersect in the flow, creating a probe volume. When particles suspended in the working fluid intersect this probe volume, light is scattered with frequencies that are mathematically related to the velocity of the fluid in the probe volume. The drawing that follows shows the general setup and flow of data. The system is capable of detecting negative velocities because

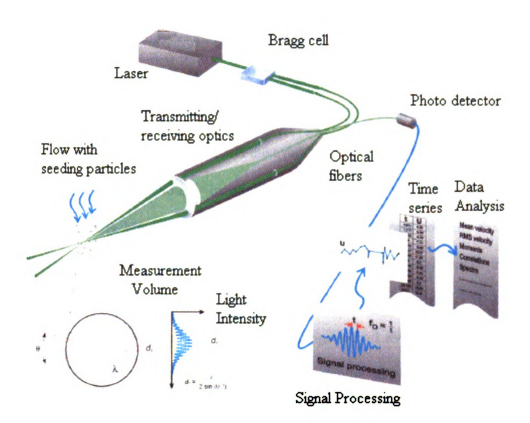


Figure 21: LDA schematic (shown in back-scatter configuration) [16].

a Bragg cell is used to shift the frequency of one of the laser beams. The forward-scatter configuration was chosen to achieve higher data rates. In forward-scatter, the detector is separate from the transmitting probe as opposed to back-scatter, where the detector is integrated in the probe.

The setup used in this experiment consisted of transmitting and receiving probes with focal lengths of 310 mm and 400 mm respectively. The dimensions of the resulting probe volume were 77 x 77 x 945 μm. These dimensions result in a probe volume of 0.004198 mm³ in a fused quartz tube. The details of this calculation are presented in Appendix B. The cross-section of the probe volume was 0.081407 mm² as compared to the quartz tube cross-sectional area of 6.9279 mm². More importantly, the length of the probe volume is approximately one third of the quartz tube's inner diameter. This

comparison was important to determine if the velocity readings could be approximated as centerline velocities. It was determined from previous experiments that the optimal angle for the receiving optics was 39° off-axis angle [9]. The fringe spacing was 3.15 µm, the frequency shift was 40 MHz, and the cyclic length was set to 360°.

Several of the previously mentioned parameters are entered into the Dantec program called PDA Flow and Particle Software. This program controls the detector settings, initiates and terminates data collection, and has several useful post-processing features. The software also requires a bandwidth. For this experiment, 1.20 MHz was chosen because it corresponds to a velocity range of -1.890 m/s to +1.890 m/s. Preliminary tests indicated that the peak velocities would fall within this range. Two parameters that can be modified to improve data collection rates are the High Voltage parameter and the Data Validation number. High Voltage corresponds to the voltage supplied to the photomultipliers. In effect, it controls the detector sensitivity. The High Voltage used for data collection ranged from 700 to 800 Volts. Too low of a voltage results in a low data collection rate, and too high results in excessive noise. The Data Validation value corresponds to the way the data is filtered. The signal/noise validation value typically varied from -1dB to 1dB.

Once these values were set, the experiment could then be run and data collected. The program was set up so that it outputted arrival time, cycle time (0-200 ms), the corresponding crank angle (0-360°), and velocity. These values were tabulated and could be exported for further analysis in Microsoft Excel or C++. The Dantec program also outputted a cycle-averaged plot, and the number of data points collected at each crank angle was tabulated. This was particularly useful for determining if the resolution

was good throughout the injection event. The cycle-averaged plot was helpful for getting an idea of the injection profile immediately. In another window, a histogram showed the total distribution of data points collected over the 200 ms event. There was also a table that showed the validation data rate, velocity validation, elapsed time, and reset pulses. The velocity validation rate roughly indicated the time resolution of the run. In order to get a velocity reading for nearly every millisecond, a validation data rate of greater than or equal to 2 kHz was required. The velocity validation feature was enabled to achieve more accurate results. Velocity validation values of 95-100% were achieved during these experiments. The elapsed time simply recorded the length of the data collection and the reset pulses indicated the number of injections collected.

3.3 Post-processing

Initially, post-processing was done in Excel. The data was sorted and the mass injected per cycle was calculated using a plug flow assumption. When it was determined that this should be done on a large scale and that the unsteady equations should be used for analysis, a program was developed in C++ to handle this task and was described in Chapter 2. In order to validate the accuracy of this program, a simpler test data set was constructed and evaluated using Excel. Brereton's program in FORTRAN was also run for comparison purposes. The C++ program showed good agreement with these programs, so it was accepted and used for analysis. To verify that the equations were reasonable, cycle-averaged results from a mass balance were compared to the predicted values outputted by the program. To begin this procedure, the mass balance was first zeroed. Fifty injections were collected in a beaker on the mass balance, and the resulting

mass was divided by fifty to determine the average mass injected per injection. When this number was compared to the output data of the C++ program, it was found to be within 6% for Injector #1 and 8% for Injector #2. This agreement will be discussed in greater detail in the next section.

CHAPTER 4

RESULTS AND DISCUSSION

4.1 Results

After perfecting the test rig and experimental procedure, tests were run using the two injectors previously introduced. The results of each injector will be discussed individually, and then a comparison of injector variability will be made at the end of this chapter.

4.1.1 Injector #1 Results

The following plots are samples of the data collected for the Toyota Prius injector.

The first plot shows an average of centerline velocity along with the voltage applied to the injector. The following plots are three individual, consecutive injection events.

Lastly, a bar graph shows the variability in the mass injected for each event.

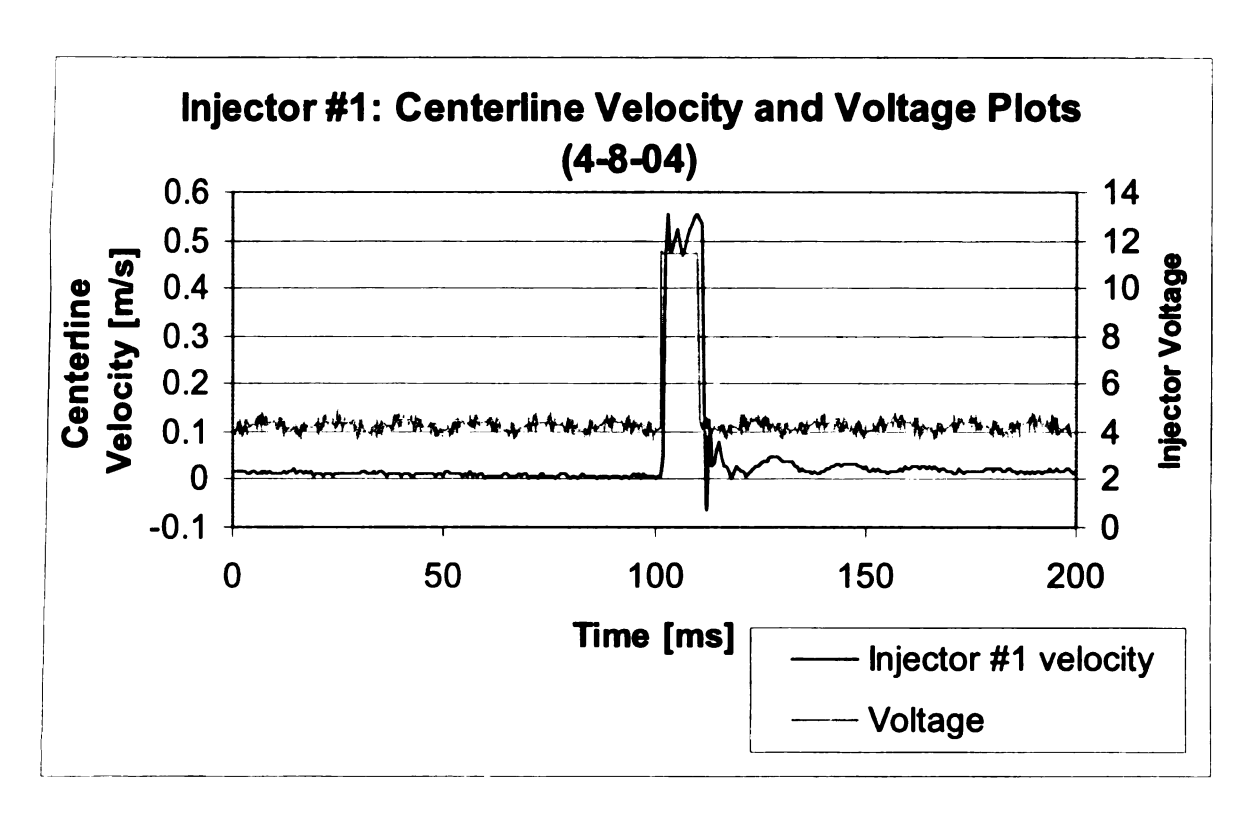
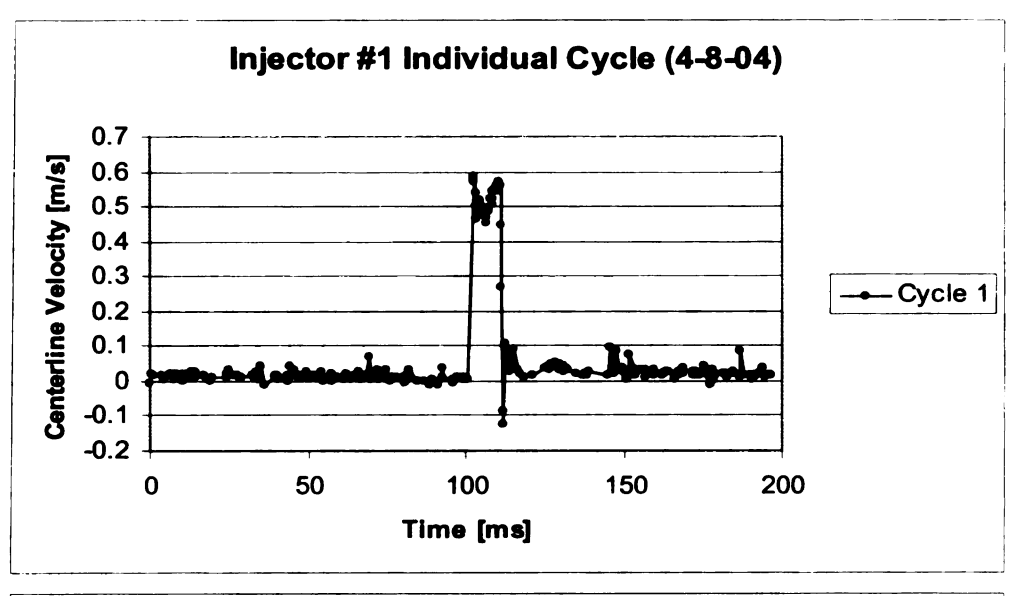
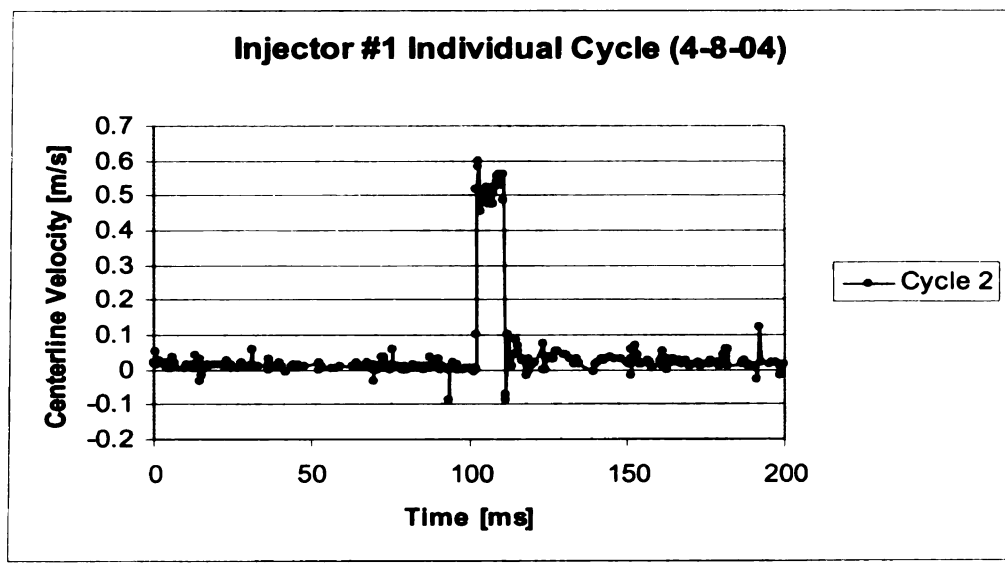


Figure 22: Cycle-averaged centerline velocity plot with injector voltage.







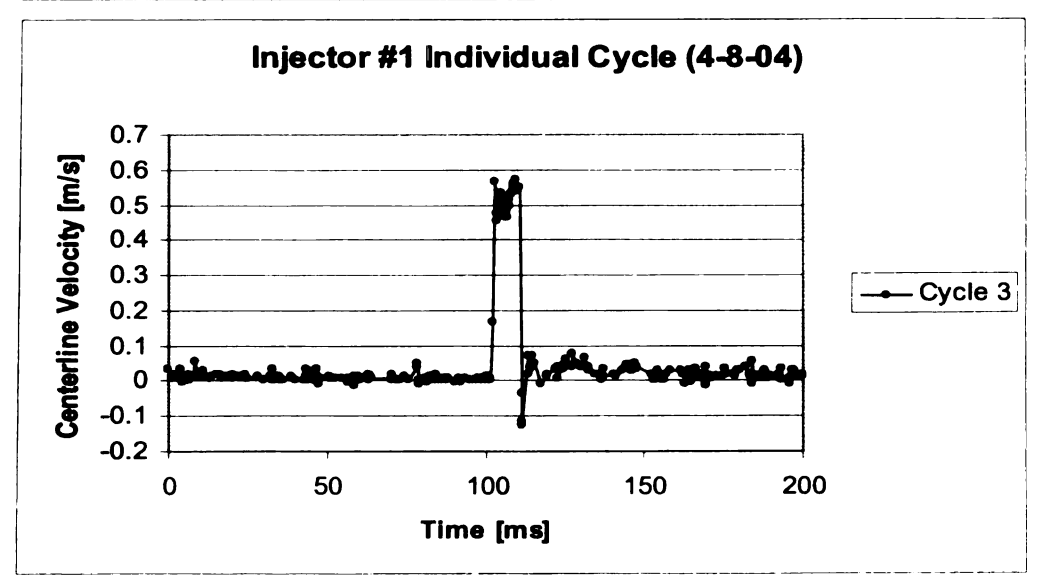


Figure 23: Three consecutive cycles from Injector #1.

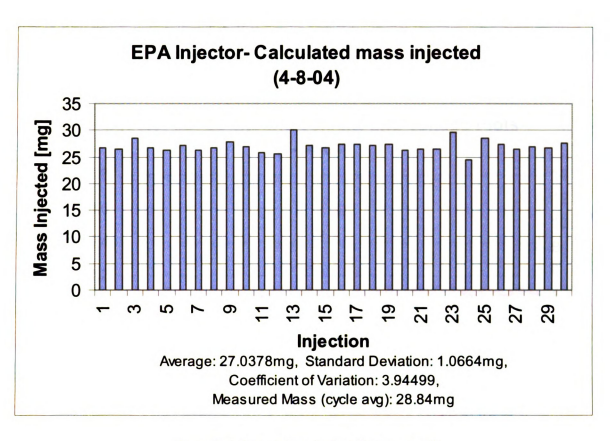


Figure 24: Mass injected chart for Injector #1.

The individual cycles show the dense distribution of data at the point of injection. The time resolution (averaging 4 data points per millisecond) gives some insight into the flow dynamics. Significant variability can be observed between the three graphs shown in Figure 23. The bar graph above shows that there is, in fact, a large amount of variability between consecutive injection events. This variation will have an effect on the fuel/air ratio, particularly for direct injection engines.

4.1.2 Injector #2 Results

The following plots are for the new Chrysler Hemi fuel injector. As before, the first plot shows an average of centerline velocity along with the voltage applied to the injector. This is followed by plots of three individual consecutive injection events and finally a bar graph showing the variability in the mass injected for each event.

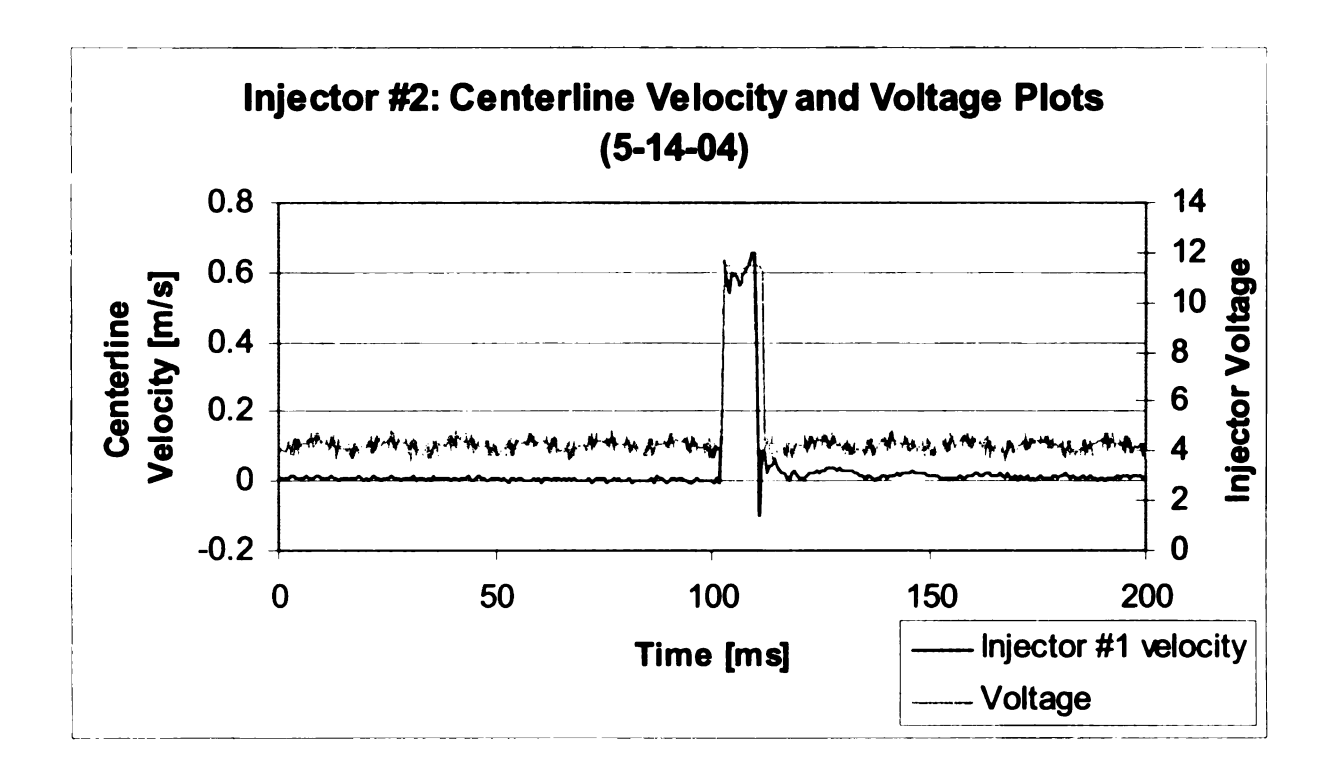
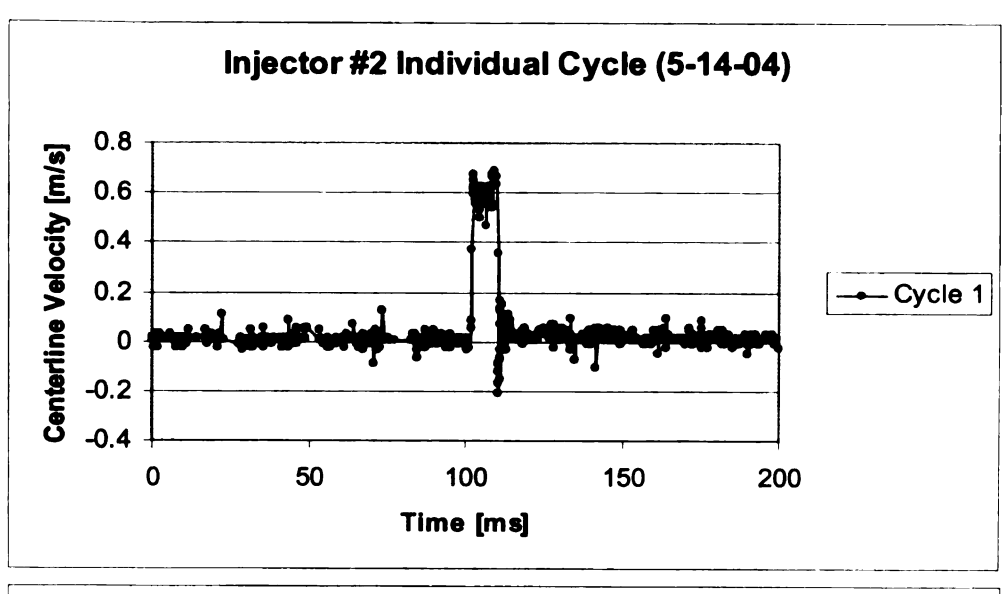
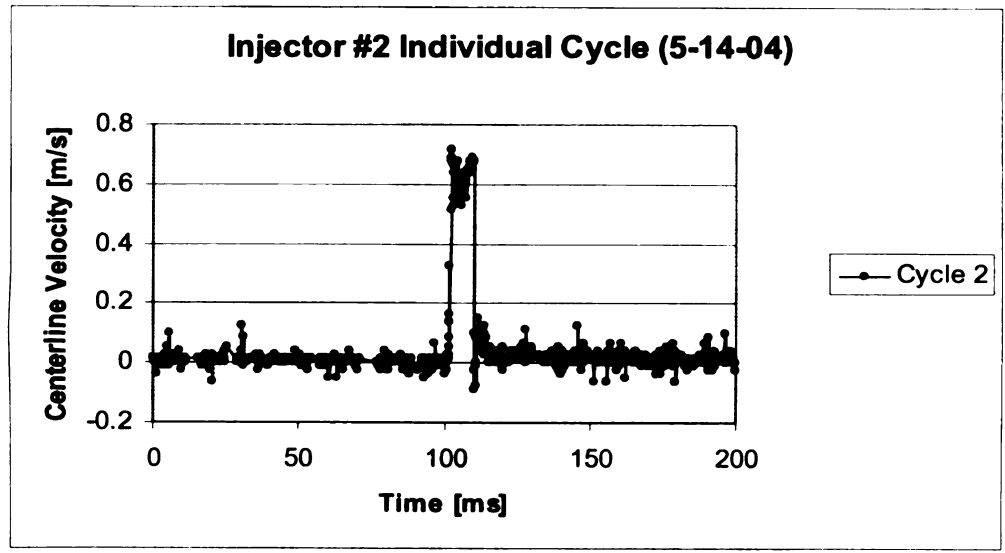


Figure 25: Cycle-averaged centerline velocity plot with injector voltage.





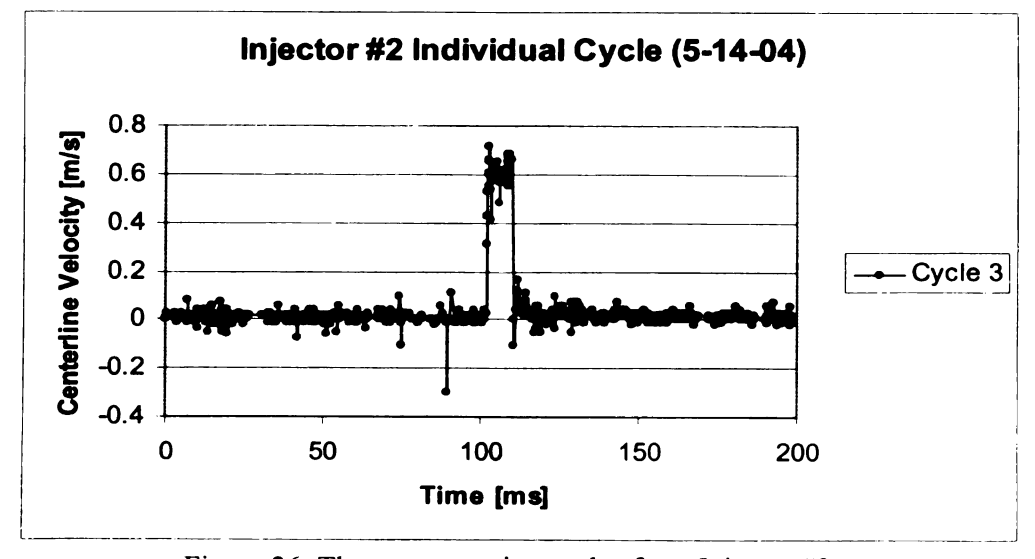


Figure 26: Three consecutive cycles from Injector #2.

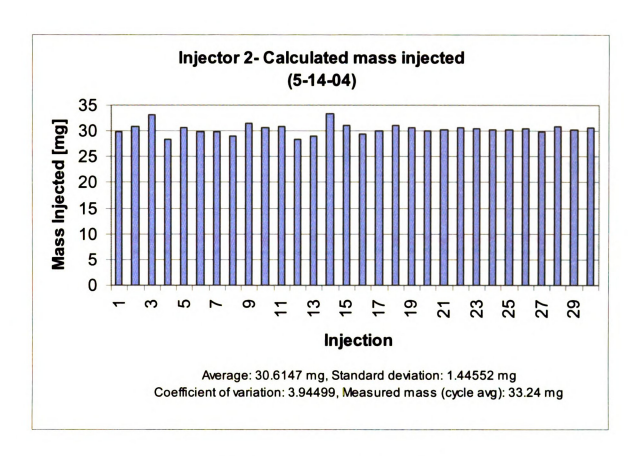


Figure 27: Mass injected chart for Injector #2.

Again, significant variability can be observed in the individual velocity traces. Initially, the bar graph shows great variability. The injector was allowed to run for several cycles before data was collected, so this variability at the beginning should not be attributed to some kind of startup condition. It is believed that this is simply a display of the varied nature of the injector. Note that the standard deviation is greater for Injector #2 than it is for the #1.

4.2 Discussion

4.2.1 Comparison of Injectors #1 and #2

Figure 28 shows the average centerline velocity plots from Injectors #1 and #2 as well as the voltage applied. It very interesting to note how similar the pressure wave

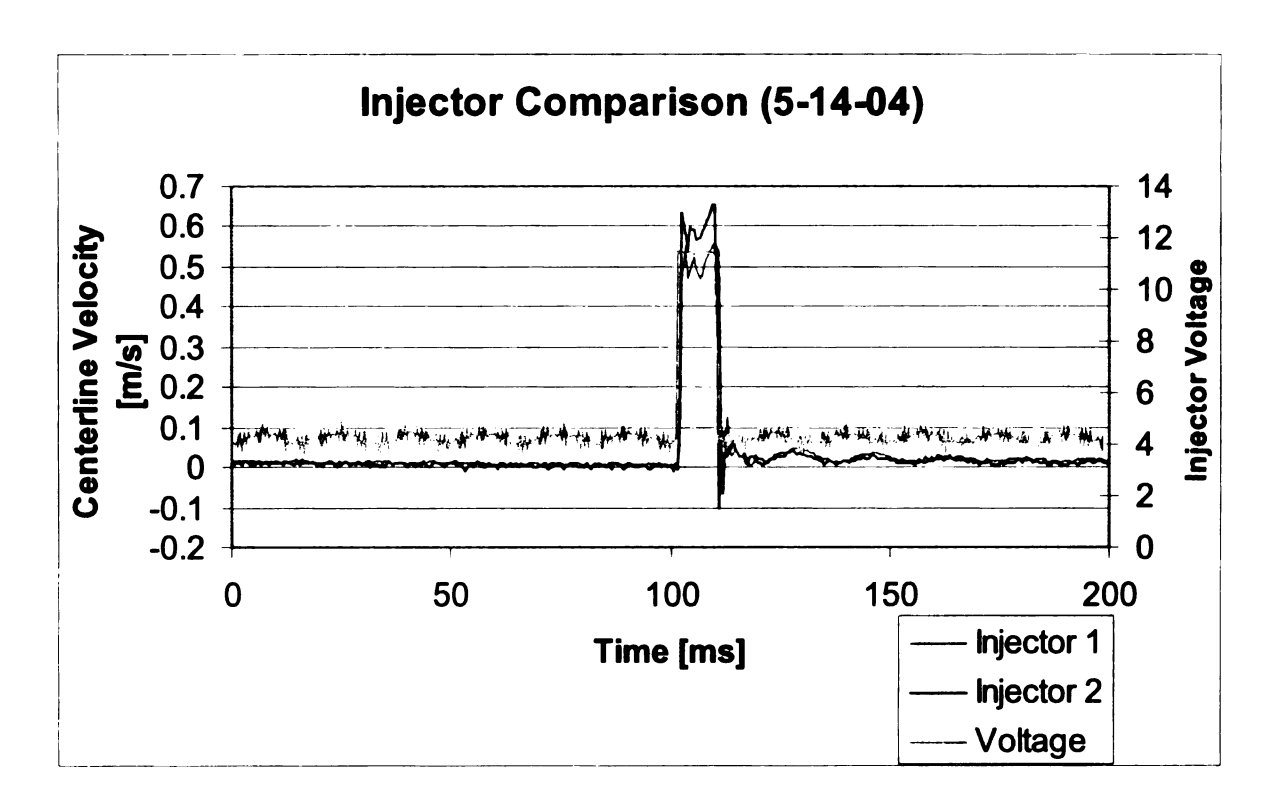


Figure 28: Average centerline velocities and applied voltage.

oscillation is. The most notable difference is that Injector #2 flows considerably more fuel. This is expected, as the cylinder displacement of a Chrysler Hemi is about twice that of the Toyota Prius.

The standard deviation of mass injected for Injector #1 was 1.0664 milligrams as compared to 1.4552 milligrams for Injector #2. It appears as though the Prius injector was designed with more precise fuel control in mind. This is not surprising because the Prius is a car whose designers were concerned with fuel economy. Also plotted are plots of the probability density functions.

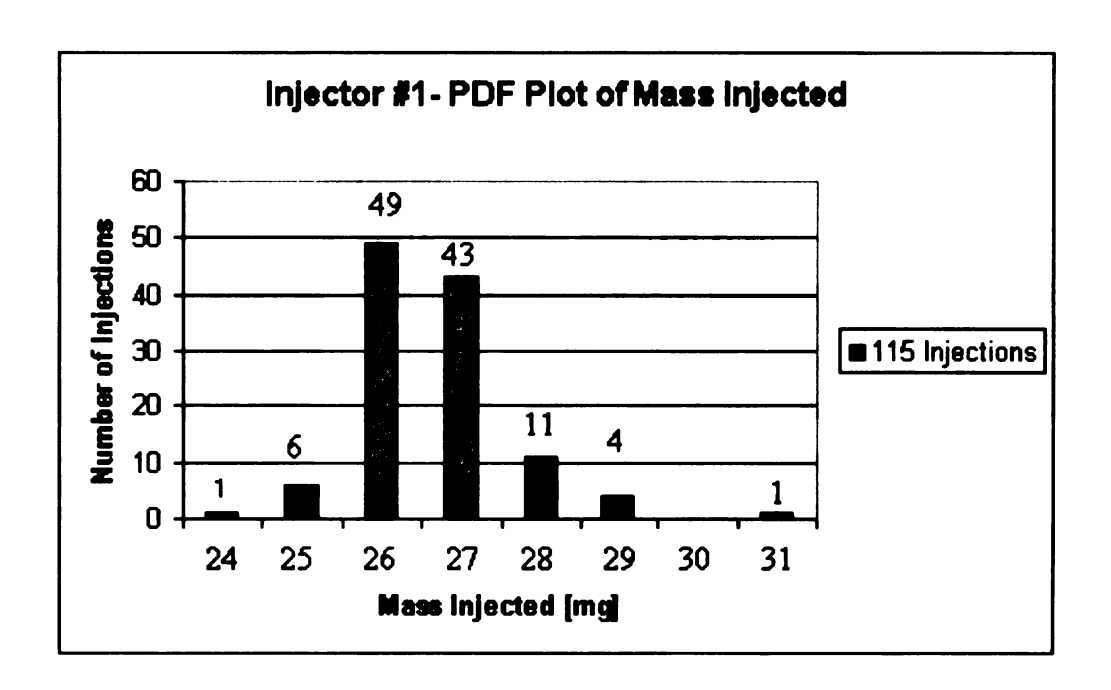


Figure 29: PDF of mass injected for Injector #1.

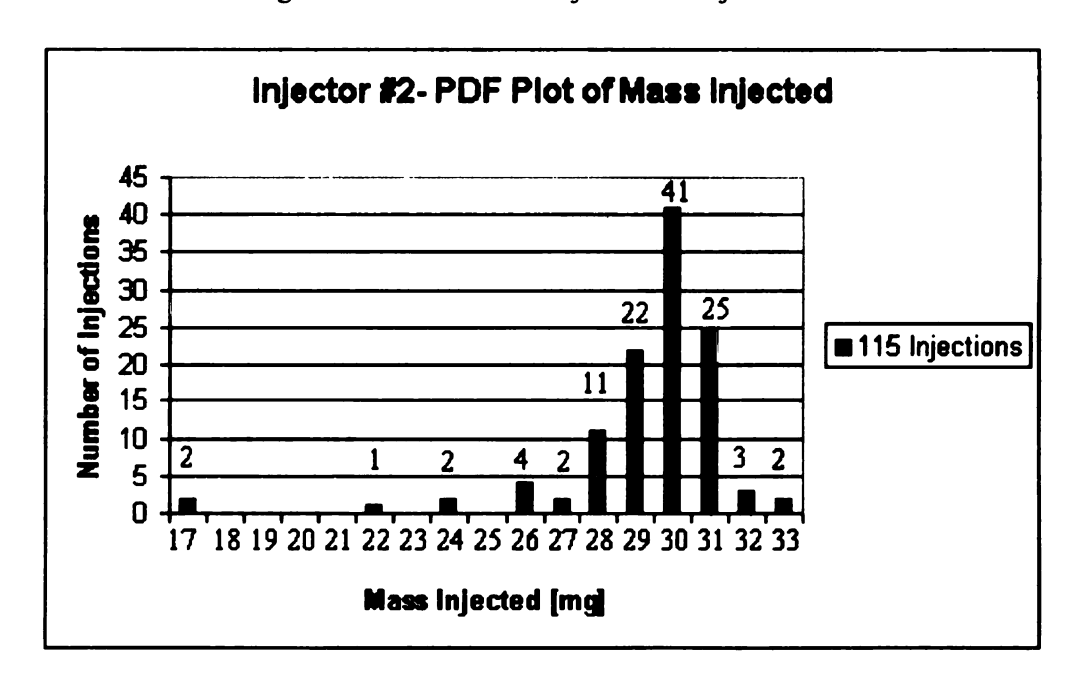


Figure 30: PDF of mass injected by Injector #2.

A useful way of viewing the injector precision is to assume that this injector variability could translate into fuel/air ratio variability. If the average were taken to be the amount of fuel required for a stoichiometric mixture, then the maximum and minimum fuel/air ratios would be as follows. This is a large range and would be highly

Table 2: Fuel/Air ratio range.

	Injecto 1	r Injector 2
Max	15.54	15.85
Min	13.27	13.48

undesirable from an emissions and fuel economy standpoint. For port injection systems, however, the fuel/air ratio may not fluctuate quite as much. There is a phenomenon whereby the fuel film on the intake runner, port, and intake valve serves as a cycle-to-cycle filter. In other words, the extreme variations in fuel injected may not result in sharp variations in the in-cylinder fuel/air ratios for port injection systems [7],[10]. This is not the case for direct injection gasoline engines, however. These engines require precise fuel metering for smooth operation. Variation in the amount of fuel injected can also have dramatic effects on the emissions produced, particularly oxides of nitrogen (NOx) and hydrocarbons (HC).

4.2.2 Sources of Variability

4.2.2.1 Cosworth Variability

A great deal of effort was taken to isolate the injector so that only the variability of the injector would be measured. Nevertheless, there is still the possibility of variability from the Cosworth control module. To investigate this, the control module was monitored using an oscilloscope to measure and plot the voltage. Three injection events are shown in the following figure. One can observe slight variations in the peak voltage. To better quantify this variability, a table was constructed from the statistics

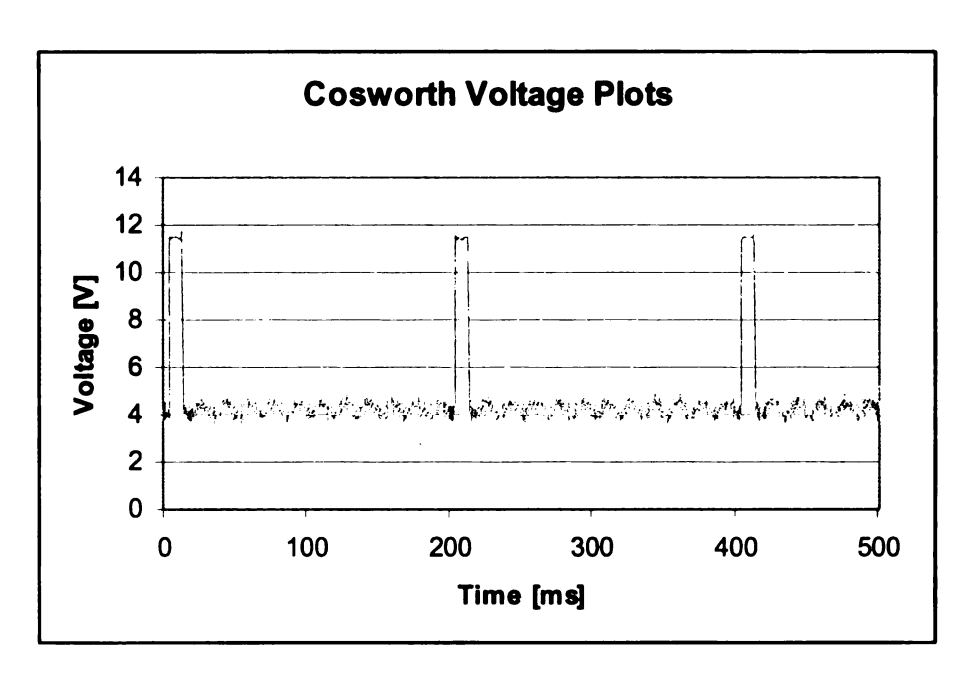


Figure 31: Voltage plot of the injection control system.

recorded by the oscilloscope. These values were recorded over a series of about 200 injection events. It would be interesting to find out if this variability had any effect on the motion of the needle inside the injector. It is possible that this variability

Table 3: Injection control system variability statistics.

		Standard Deviation	Minimum	Maximum
Volts peak-to-peak	7.965 V	111 mV	7.87 V	8.92 V
Period	199.998 ms	32 μs	199.61 ms	200.03ms
Frequency	5.0004 Hz	794.459 μHz	4.9994 Hz	5.0098 Hz
Rise Time	442 μs	224 μs	320 μs	2.15 ms

had an affect the performance of the injector. For that reason, the variability presented should be considered the variability of the injector and the control module.

4.2.2.2 Sources of Error

As with any experiment, there is always the potential of errors affecting the end result. The uncertainty errors and systematic errors associated with this experiment will be discussed at this time.

Uncertainty errors in this experiment arose from the measurements of the quartz tube diameter, centerline velocity, as well as the temperature measurements needed to determine the fluid density. Recall that the general form of the equation used to solve for the mass flow rate was

$$\dot{m}(t) = \rho \cdot (\pi \cdot R^2) \cdot U(t) \tag{4}$$

where

$$U(t) = \frac{1}{2}u_{cl}(t) + \frac{d}{dt}(u_{cl}(t)) * W(t) . (5)$$

The uncertainty associated with the quasi-steady portion $\left(\frac{1}{2}u_{cl}(t)\right)$ is given by taking the partial differential of (4) using the following equation

$$d\dot{m} = \frac{1}{2} [(\rho \cdot u \cdot dA) + (\rho \cdot A \cdot du) + (A \cdot u \cdot d\rho)]. \tag{7}$$

The uncertainty from the radius measurements is ± 0.005 mm, from the velocity measurements (LDA precision) ± 0.0005 m/s, and from the density ± 0.05 kg/m³. The resulting uncertainty from this quasi-steady calculation is ± 0.001839 mg/ms. To put that into perspective, the quasi-steady mass flow rates varied from 0 to 2.07416 mg/ms. Thus, the uncertainty contributions from measurements and tabulated values were quite low.

Systematic errors are likely present, though their direct contributions may be more difficult to quantify. One key assumption that was made was that the quartz tube was

perfectly circular and that it had a uniform cross-sectional area throughout its length.

Obviously the calculations are quite sensitive to the diameter measurement as it is squared in the area calculation.

There are also some errors associated with measuring the centerline velocity. As previously stated, the recorded velocities were assumed to be centerline velocities. In reality, these are the probe volume-averaged velocities. While the probe volume area is small compared to the flow area, the length of the probe volume is approximately 1/3 of the diameter. This could contribute to some error as a result of this averaging. With the assumed parabolic profile, it is reasonable to assume that the error in the measured velocity introduced as a result of the probe volume is 0-5%. A key parameter that affects the accuracy of the velocity is the measurement of the angle between the laser beams. Based on previous experiments, the velocity is likely affected by this parameter by about \pm 2%. Finally, processing error could also come into effect. The documentation on the LDA system indicated that the processor accuracy was \pm 0.5% full spectrum. Since the velocity range was from -1.2-1.2 m/s, this translates to 0.006 m/s. It is likely that these errors would average out since several tens of thousands of samples were taken. While these certainly are not all the potential sources of error, they were thought to be the major contributors.

Having discussed the potential sources of error, however, it should be understood that for the experiments run, the agreement was very good with the cycle-averaged measurements. The table on the following page shows this agreement. The LDA measurements of the mass injected by Injector #1 was typically within 6% and Injector #2 within 8% of the cycle-averaged measured values from the mass balance. Moreover,

the relative cycle-to-cycle variability shown by the previous bar graphs is unaffected by this uncertainty. The only change is in the magnitude of the mass injected. The reason for this is that the calculation procedure for the mass injected for each cycle is the same and the LDA equipment was not moved between measurements. Any error present should be consistent.

Table 4: Comparison between mass balance and LDA measurements

Injector #1				Injector #2			
Mass Balance Measurement (mg)	LDA Injection Average (mg)		1	Mass Balance Measurement (mg)	LDA Injection Average (mg)		
28.84	27.343	5.191		33.24	30.7676	7.438	
28.84	27.2857	5.389		33.24	30.4943	8.260	
28.84	27.0378	6.249		33.24	30.6147	7.898	

CHAPTER 5

CONCLUSIONS

In this study, the real time cycle-to-cycle variability of a fuel injector and its control system was quantified. The approach was quite different from traditional measurement techniques as it involved measuring the centerline velocity *before* the injector using LDA as opposed to making measurements *after* the injector. It was also found that good time resolution is necessary, and the seed used to scatter the laser light must not plug the injector if the results are to be trusted.

The results of these experiments have shown that there is a significant amount of cycle-to-cycle variation for the two injectors used. The Toyota Prius injector (Inj. #1) had an observed standard deviation of 1.0664 mg while that for the Chrysler Hemi (Inj. #2) injector was 1.4552 mg. If the variability in mass injected was directly related to the fuel/air ratio, this would result in a large amount of variation and would be highly undesirable for clean, efficient combustion. For port injection systems, this may not be the case because of fuel film that is a result of wetting on the valves and/or intake ports. This causes a filtered or damped response so that the actual fuel/air ratio seen in the cylinder may not show as much variability as the fuel injector [7],[10]. In the case of directly injected engines, however, this variability is much more closely related to the incylinder fuel/air ratio. There have also been some recent developments in fuel-injected two-stroke engines. More precise electronic fuel control could make these engines cleaner and more acceptable in the near future [17]. The measurement technique outlined



in this report could prove to be a useful tool for companies striving to design more precise and consistent fuel injector performance for such applications.

While developing and perfecting this measurement method, several important discoveries were made. These discoveries are discussed in detail in Appendix C and will be summarized at this time.

First, the microbubble seeding technique used in this experiment proved to be extremely effective. By introducing thousands of these tiny bubbles into the working fluid, excellent data rates were achieved without plugging the fuel injector. Because of the small size of these bubbles, they did little or nothing to affect the velocity profile and bulk fluid density (proved experimentally).

The second useful discovery was the presence of air in the fuel injector and the effects it has on the centerline velocity. Figure 30 shows the difference in the centerline velocity profile with and without air in the injector. These oscillations affect the

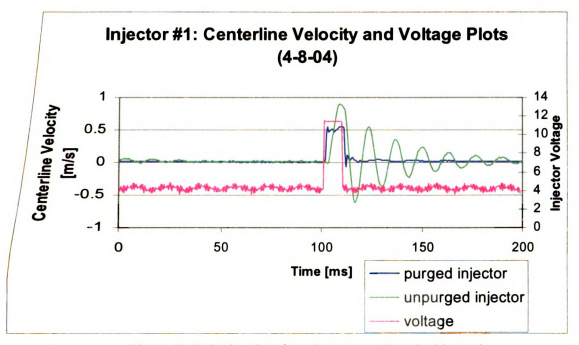


Figure 32: Velocity plots for Injector #1 with and without air.

consistency of the injector. In some cases, the oscillation did not die out before the next injection event, adding to injector variability. Even though it was initially thought that these bubbles would dissolve or "work themselves out" of the system, this was not observed over the course of several days of intermittent testing.

Lastly, it was determined that a fuel injector is only as good as the control system that actuates it. If there are fluctuations in the voltage sent to the injector, increased variability is inevitable. Stable control systems must be developed to minimize this problem.

CHAPTER 6

RECOMMENDATIONS

After completing this project, it was clear that there were several other areas that would be worth to investigating.

- Use gasoline in test rig and automotive injection control unit as well as stock fuel delivery setup to simulate more realistic conditions. Is there any variability introduced by the addition of a fuel pump? How much?
- Find a way to quantify the variability of the injector with air inside. How much of an improvement is there when the air is evacuated?
- Evacuate air from injectors in an engine on a dynamometer/emissions test cell to see how performance and emissions changes as a result.
- Measure variability in high-pressure diesel injectors. It is difficult to design a
 quartz window that can withstand these high pressures. Such a window has
 already been developed here at the Michigan State University Engine
 Research Laboratory, however. This window has been tested up to about
 30,000 psi [8].
- Streamline software for sale to companies which develop fuel injectors for commercial use.
- Compare similar injectors made by the same company to measure variability from one injector to another. Is the manufacturing process consistent enough?
- Measure variability in a piezoelectric injector (Siemens). Are they more consistent? What is the consistency for multiple injection systems?

• Test injectors for DI, HCCI engines. Since there is no wall-wetting filtering effect, precise fuel metering is more important.

Great strides have been made in fuel injection technology since the 1920's, but there is still much more that can be explored in this field. More precise fuel injectors and control systems will enable automotive manufacturers to achieve greater fuel efficiency and cleaner emissions than ever before.

Appendices

APPENDIX A

Details of the Mass Flow Equation

The exact unsteady solution of the laminar Navier-Stokes equations is discussed in this section as developed by Brereton [14]. As previously mentioned, the general expression for calculating the mass flow rate in uniform density flow is

$$\dot{m}(t) = \rho \cdot (\pi \cdot R^2) \cdot \overline{u}(t) \tag{4}$$

and, in unsteady developed pipe flow,

$$\overline{u}(t) = \frac{1}{2}u_{cl}(t) + \frac{d}{dt}(u_{cl}(t)) * W(t)$$
 (5)

where W(t) is a known weighting function and * the convolution operator. This exact solution applies to laminar, fully developed, constant property duct flow undergoing arbitrary unsteadiness from an initially steady state. Recall that the $\frac{1}{2}u_{cl}(t)$ term is simply the momentary velocity term for a steady laminar parabolic velocity profile. The $\frac{d}{dt}(u_{cl}(t))*W(t)$ term is an unsteady correction term. By definition of the convolution operator *,

$$\frac{d}{dt}(u_{cl}(t))*W(t) = \int_{0}^{t} \frac{du_{cl}}{dt}(t-t') \cdot W(t') \cdot du$$
 (7)

For simplicity of evaluation, the following non-dimensional term is now introduced:

$$\tau = \frac{v \cdot t}{R^2} \,. \tag{8}$$

Here, v is viscosity, t is time, and R is the measurement tube radius. $W(\tau)$ is an inverse convolution integral term which can be described as follows:

For
$$\tau < 0.01$$
, $W(\tau) = 0.5 - 2.2567\sqrt{\tau} + 1.125\tau$ (9)

$$e^{-44.73179\tau} \left(0.253393 \cos(26.1288\tau) + 0.499595 \sin(26.1288\tau) \right) + e^{-171.40560\tau} \left(0.0816947 \cos(58.5689\tau) + 0.289019 \sin(58.5689\tau) \right)$$
For $\tau \ge 0.01$, $W(\tau) = + e^{-377.58150\tau} \left((0.0402422 \cos(94.0270\tau) + 0.200663 \sin(94.0270\tau) \right) + e^{-662.97270\tau} \left((0.0240313 \cos(131.510\tau) + 0.153211 \sin(131.510\tau) \right) + e^{-1027.47400\tau} \left((0.0160209 \cos(170.521\tau) + 0.123770 \sin(170.521\tau) \right)$

as given in Brereton, Schock, Rahi, and Bedford [15].

In this solution, the angles are in radians. Once this "modified" area-averaged velocity in (5) is developed from the measured centerline velocity history, the mass injected can then be calculated by carrying out the convolution integral, at each instant in the time series, and multiplying $\bar{u}(t)$ by the fluid density and the cross-sectional area of the tube. It was determined that the unsteady correction term contributes nearly as much (~45%) to the calculation of the total mass injected as the quasi-steady laminar parabolic profile portion.

APPENDIX B

Calculation of the LDA Probe Volume

In an LDA system, two laser beams cross in a fluid flow. The drawing below shows the general layout of an LDA system and shows the ellipsoidal shape of the probe volume. The intersecting lasers produce a series of fringes. As particles cross this

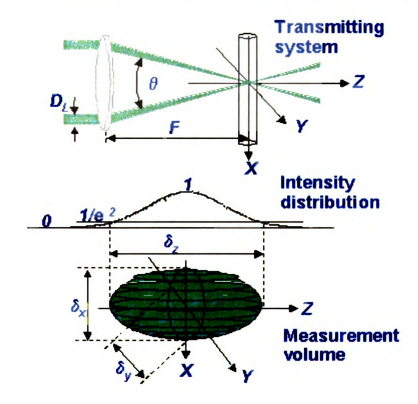


Figure 33: Probe volume diagram and intensity distribution [16].

probe volume, light is scattered. The fluid velocity can then be determined based on the Doppler shift of the light reflected from the moving particle.

When calculating the probe volume, the following diagram and equations are very useful.



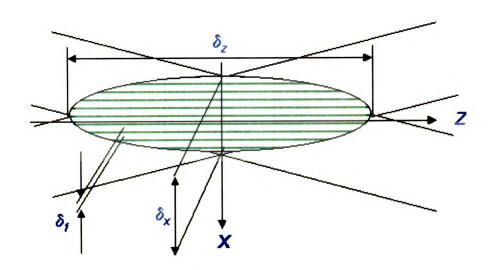


Figure 34: Probe volume dimensions [16].

Length:
$$\delta_z = \frac{4F\lambda}{\pi \cdot ED_L \sin\left(\frac{\theta}{2}\right)}$$
 (10)

Width:
$$\delta_{v} = \frac{4F\lambda}{\pi \cdot ED_{L}} \tag{11}$$

Height:
$$\delta_z = \frac{4F\lambda}{\pi \cdot ED_L \cos\left(\frac{\theta}{2}\right)}$$
 (12)

Fringe separation:
$$\delta_f = \frac{\lambda}{2\sin\left(\frac{\theta}{2}\right)}$$
 (13)

Number of fringes:
$$N_f = \frac{8F \tan\left(\frac{\theta}{2}\right)}{\pi \cdot ED_L}$$
 (14)

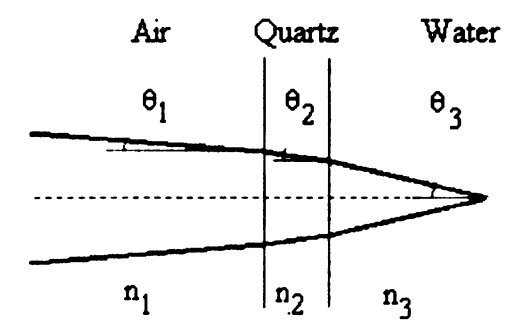
Table 5: Probe volume variables.

Variable	Description	Experimental Value
F	focal length	310 mm
λ	wavelength	514.5 nm
θ	beam angle	4.684
E	expander ratio	1.95
DL	diameter of laser	1.350 mm

When the test fluid is air, these equations can be used as they are. For the case of fluid flowing through a quartz tube, refraction must be considered. The refractive index of quartz and the working fluid, water in this case, must be known and the effective beam angle must be modified according to the following equation:

$$n_1 \sin_i = n_2 \sin \theta_i \tag{15}$$

In this equation, n is the refractive index of the medium, i stands for incidence, and t stands for transmitted. The following diagram shows how the angle changes as it passes through each medium. Now that all the variables are known, the dimensions can be



	Refractive
Material	Index
Air	1.0002926
Water	1.33157
Fused Quartz	1.45843

Figure 35: Beam refraction sketch and values.

calculated and finally the probe volume, using the equation for the volume of an ellipsis shown below.

$$V_{ellipse} = \frac{4}{3}\pi \cdot \frac{dx}{2} \cdot \frac{dy}{2} \cdot \frac{dz}{2}$$
 (16)

The results are shown for calculating the probe volume in air as well as inside a quartz tube with water.

Table 6: Results of probe volume calculations.

Dimension	Value in air	Value in quartz tube/water
δy (mm)	0.077217	0.077217
δχ	0.077475	0.077345
δΖ	0.945584	1.34233
Volume (mm^3)	0.002926	0.004198
Fringe Separation (μm)	3.15	3.15
Number of Fringes	24	24



APPENDIX C

Evolution of Experimental Technique

Over the course of this project, several discoveries were made that were quite significant. This section discusses these discoveries and the lessons learned from them.

Fuel Delivery Tube

Early in the experimental phase, the test rig was designed with a rubber fuel injection hose that connected to the quartz tube and supplied the injector with fuel. The working fluid was mineral spirits because it possessed a density and viscosity that was similar to gasoline but is safer to work with. The mineral spirits was then seeded with the previously mentioned Dantec polyamid seed. The initial plots looked like the one shown on the following page. After overlaying the voltage plot on top of the velocity plot, it

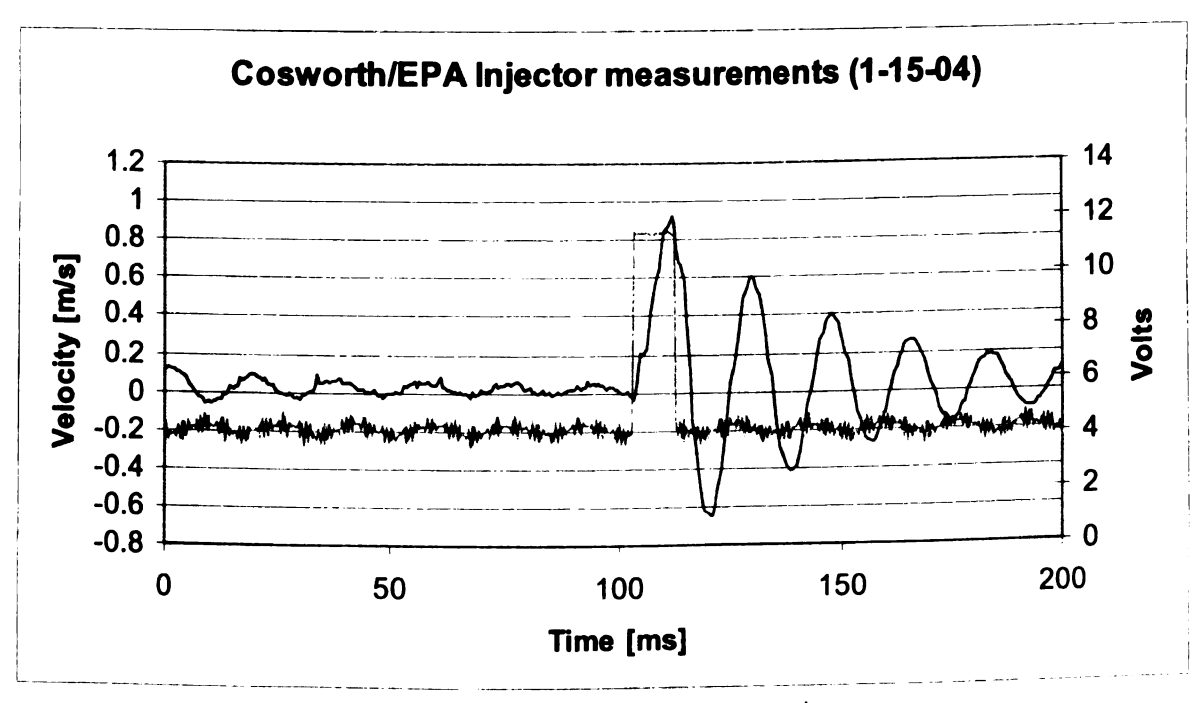


Figure 36: Average plot of early experiments.

was proposed early on that the first spike corresponded to the injector opening and that the remaining oscillations were due to pressure waves. This was later found to be partially correct. At the time, it was thought that the pressure waves reflected back to the surface of the beaker containing the fuel. However, when wave speeds were estimated using the following equation and, it was determined that the speed oscillations was far to

$$c = \sqrt{\frac{Eh}{2\rho \cdot R}} \tag{17}$$

slow. In this equation E is the Young's modulus, h is the wall thickness, p is the density of the liquid, and R is the inner radius of the tube. At that point in time, the cause of this oscillation was unclear. In order to observe the effects of pressure waves, the fuel supply line was modified. Two tests were designed: the first tube was a 20-inch rubber tube, the second a 15-inch copper tube. The resulting velocity plots are shown in Figures 35 and 36. From these graphs, it was evident that the type of fuel delivery line affects the rate and duration of oscillation. The copper tube shows the greatest amplitude and longest duration of oscillation, while the rubber tube has the smallest amplitude and shortest duration. The reason for this is that the walls of the rubber tube appear to absorb pressure fluctuations while the rigid walls of the copper tube do little to absorb them. Because the purpose of this investigation is to isolate the variability of the fuel injector, the long rubber tube is preferred. This was later changed to a clear nylon tube for viewing purposes.

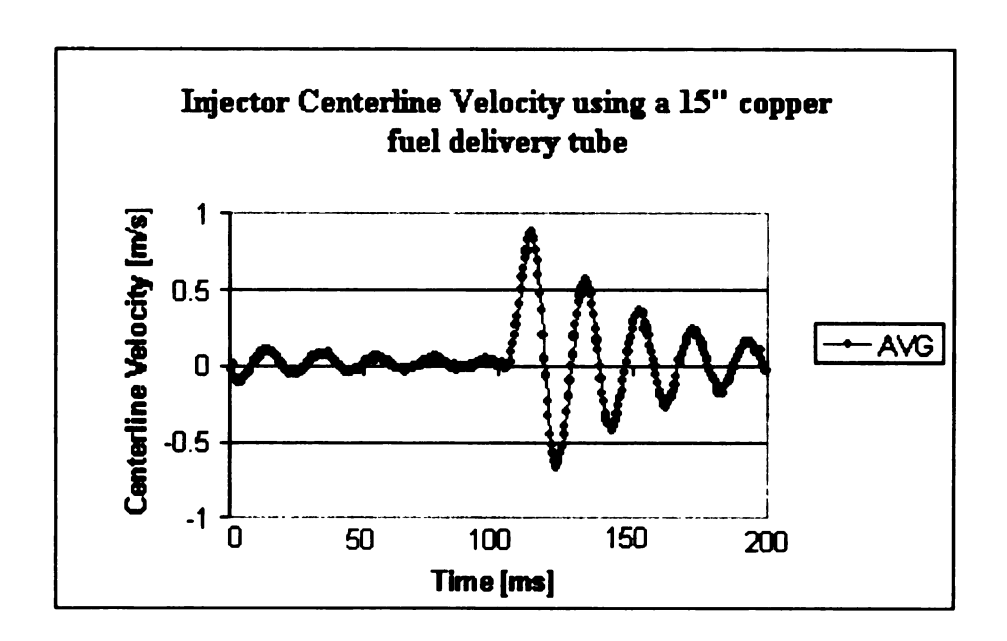


Figure 37: Velocity profiles for a 15-inch copper fuel delivery line.

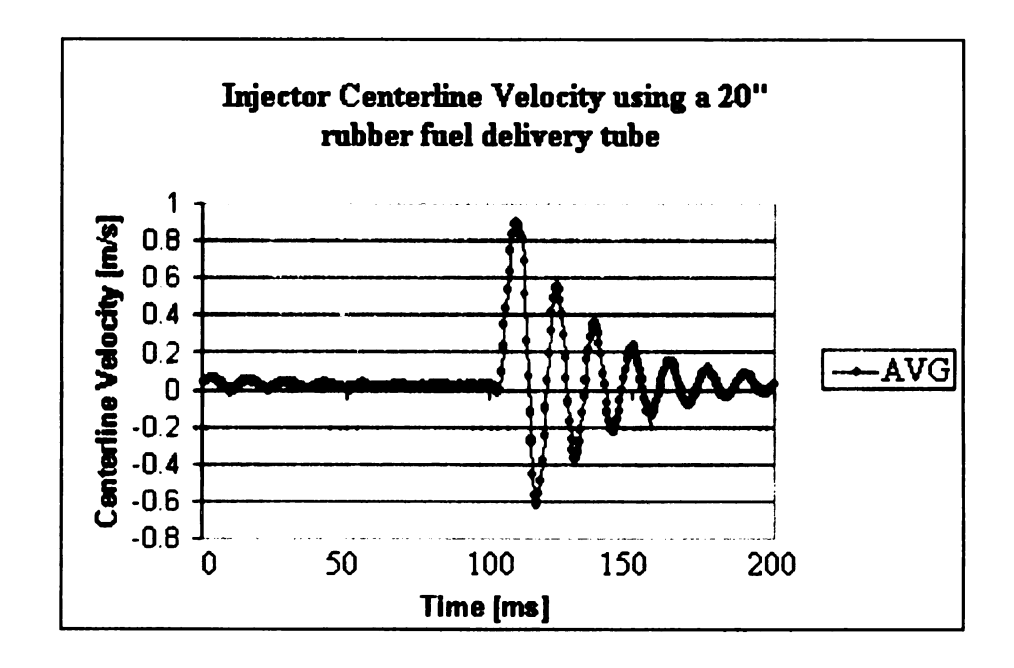


Figure 38: Velocity profile for a 20-inch rubber fuel delivery line.

Seeding

Another interesting observation was that the shape of the velocity profile had a tendency to change throughout time. Several causes were proposed. One thought was

that as the fuel beaker emptied, the distance traveled by the pressure waves was shortened. Another possible explanation was that the seed was building up in the injector and plugging it. This theory was developed after observing a thin film of seed that remained on the walls of the beaker that supplied fuel to the system. To test this theory, STP Super Concentrated Fuel Injector Cleaner was run through the injector undiluted. The cleaner was allowed to soak in the injector and then purged the following day. After cleaning the injector, data was again collected. These velocity profiles resembled earlier profiles, so it was determined that the injector was in fact plugging due to seeding the flow.

To remedy this problem, a microbubble seeding technique was devised. To accomplish this, water was placed in a high-speed blender with a small amount of concentrated liquid soap. When the blender was turned on, air was entrained and finely distributed into the water. The soap coated these bubbles and slowed down diffusion allowing the bubbles to remain suspended in the water for several minutes. This method resulted in greater data rates and much more consistent velocity profiles. The size distribution of these bubbles can be seen in the PDA bar graph that follows.

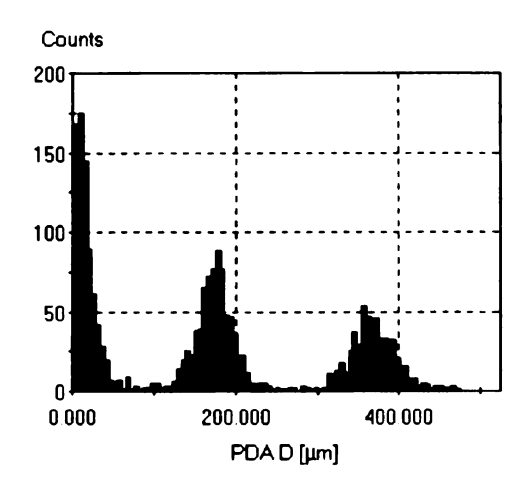


Figure 39: Bubble sizes used to seed the flow.

The following profiles show how seed eventually plugs the injector, alters the velocity profile, and how the use of bubbles remedies this problem.

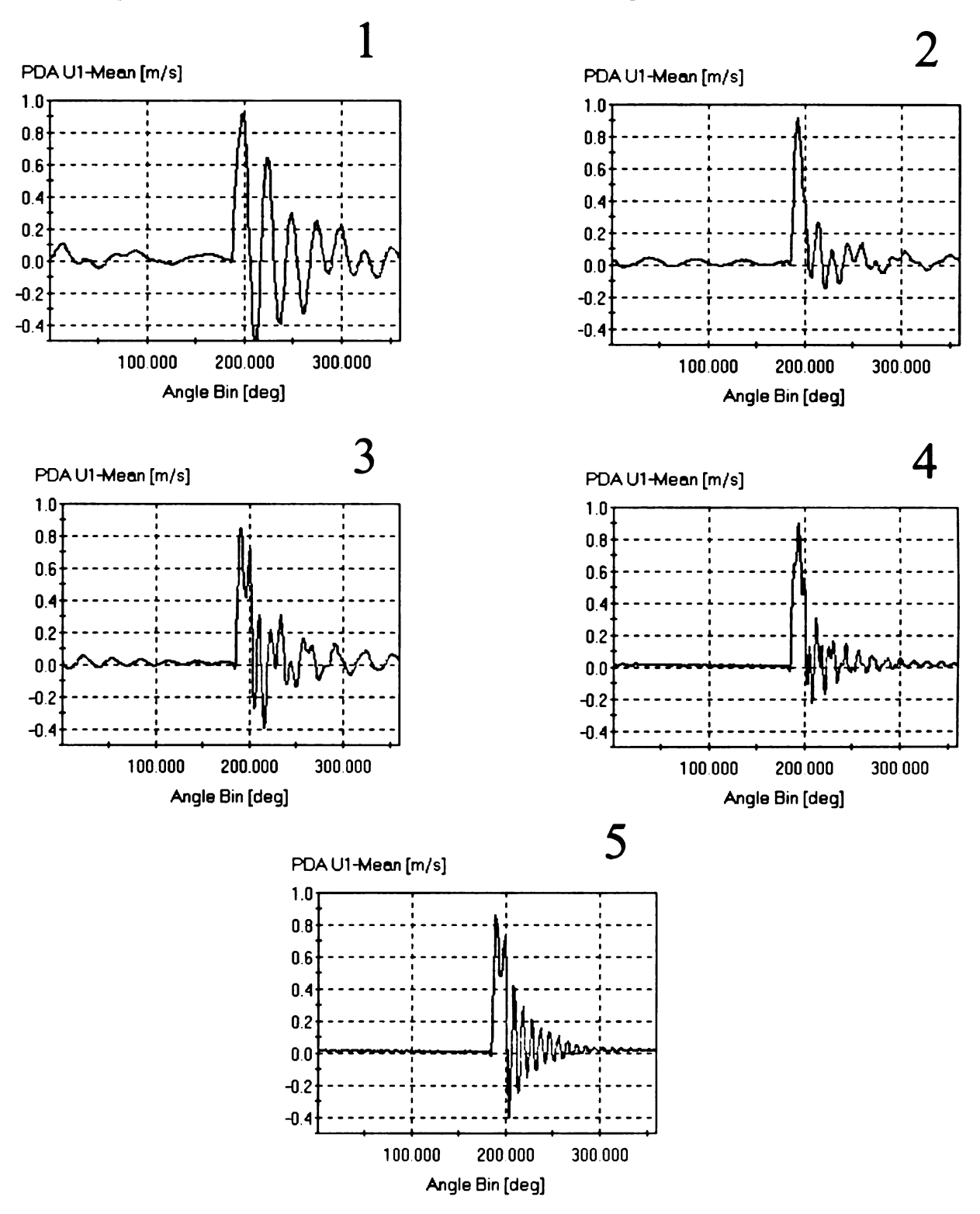


Figure 40: Velocity profiles taken through time with seed and water.

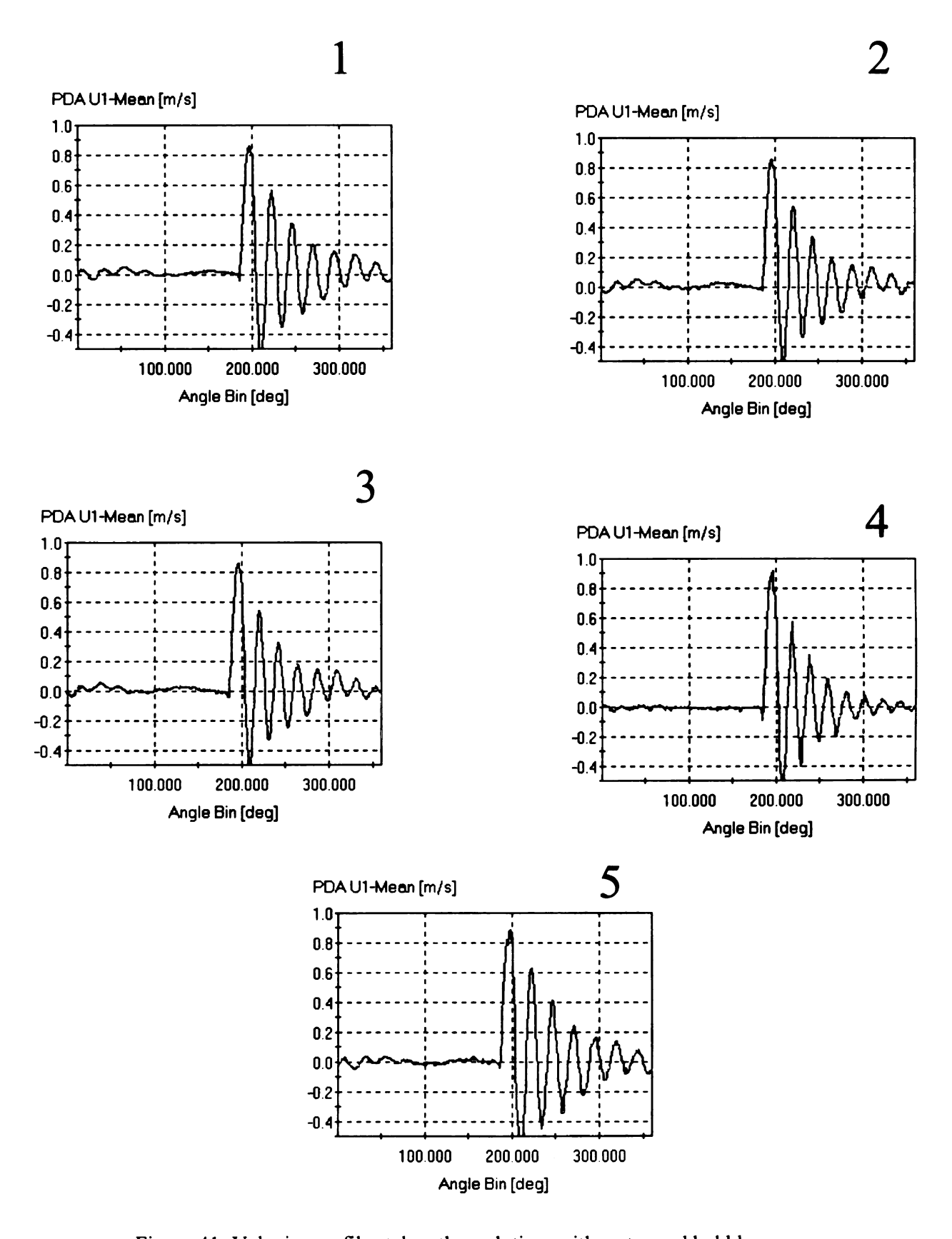


Figure 41: Velocity profiles taken through time with water and bubbles.

Air Pockets

Up until this point, mass flow calculations were performed assuming plug flow. As mentioned earlier, this assumption proved to be inaccurate and did not agree well with cycle-averaged measurements made with the mass balance (over-predicted by 60 %). Assuming the flow was quasi-steady and assuming a laminar parabolic profile was also inaccurate, under-predicting by 45%. At this point, it was determined that the flow could not be assumed as quasi-steady. The equations developed by Brereton [14] and outlined in Section 1.5 and Appendix A of this report were then employed. After the program written to perform these calculations was completed and debugged, it was run using centerline velocity data to find the mass injected per cycle. These results over-predicted the mass injected by about 30%. It was then proposed that the system might have air in the injector. The equations used determine the mass flow at the location of the centerline velocity measurement. In order to find the mass injected by the injector, it was assumed that what went into the injector must exit. Since the calculations were performed during the duration of the voltage applied to the injector, air in the injector could allow more fuel to exit than entered due to compression of the air pocket.

To test this theory, a vacuum pump was connected to the fuel line. The rubber fuel line was replaced with a clear nylon line so that air bubbles could be observed. The water was also dyed for the same reason. The system was also equipped with extra valves to facilitate the removal of air without removing excessive amounts of liquid. Once the setup was modified, the pump was turned on. It was immediately obvious that there was in fact air in the injector, as bubbles came out of the injector. This was viewed through the quartz tube. It was also clear that air tended to remain in the fuel line. After

all the air was removed from the system, new data was collected. The resulting velocity trace did not look anything like previous traces. It did, however, have a very close resemblance to the trace of the voltage applied to the injector. A plot of velocity traces with and without air in the lines is shown on the following page along with the voltage trace. The data from this run was run through the program to find the mass injected per cycle. The average outputted by the program was within 6% of the cycle-averaged measurement from the mass balance. Also, the sharp oscillation at the peak and just after the velocity returns to zero on the purged injector plot have wave speeds similar to the pressure wave speeds calculated earlier.

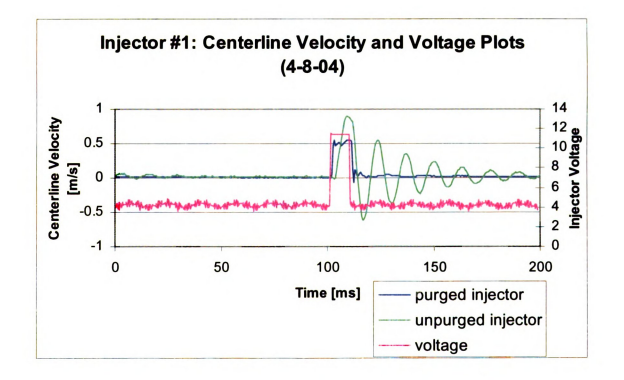


Figure 42: Velocity plots for Injector #1 with and without air.

After seeing these results, one obvious question arose: How does this air remain in the fuel injector? It does not appear that this air is simply flushed out of the injector or diffused into the water, because weeks of testing yielded the same oscillating velocity profile. Only when a vacuum was attached to the fuel line did the air come out of the injector. In order to investigate this, a spare Chrysler Hemi injector was milled to reveal the internal components and passages of the injector. The picture of this injector can be seen below. Looking at this picture, there appears to be a fairly large crevice. Further inspection reveals that this is the location where the lower nozzle portion of the injector joins with the upper portion. This could very well be the location where air pockets are trapped inside the injector.

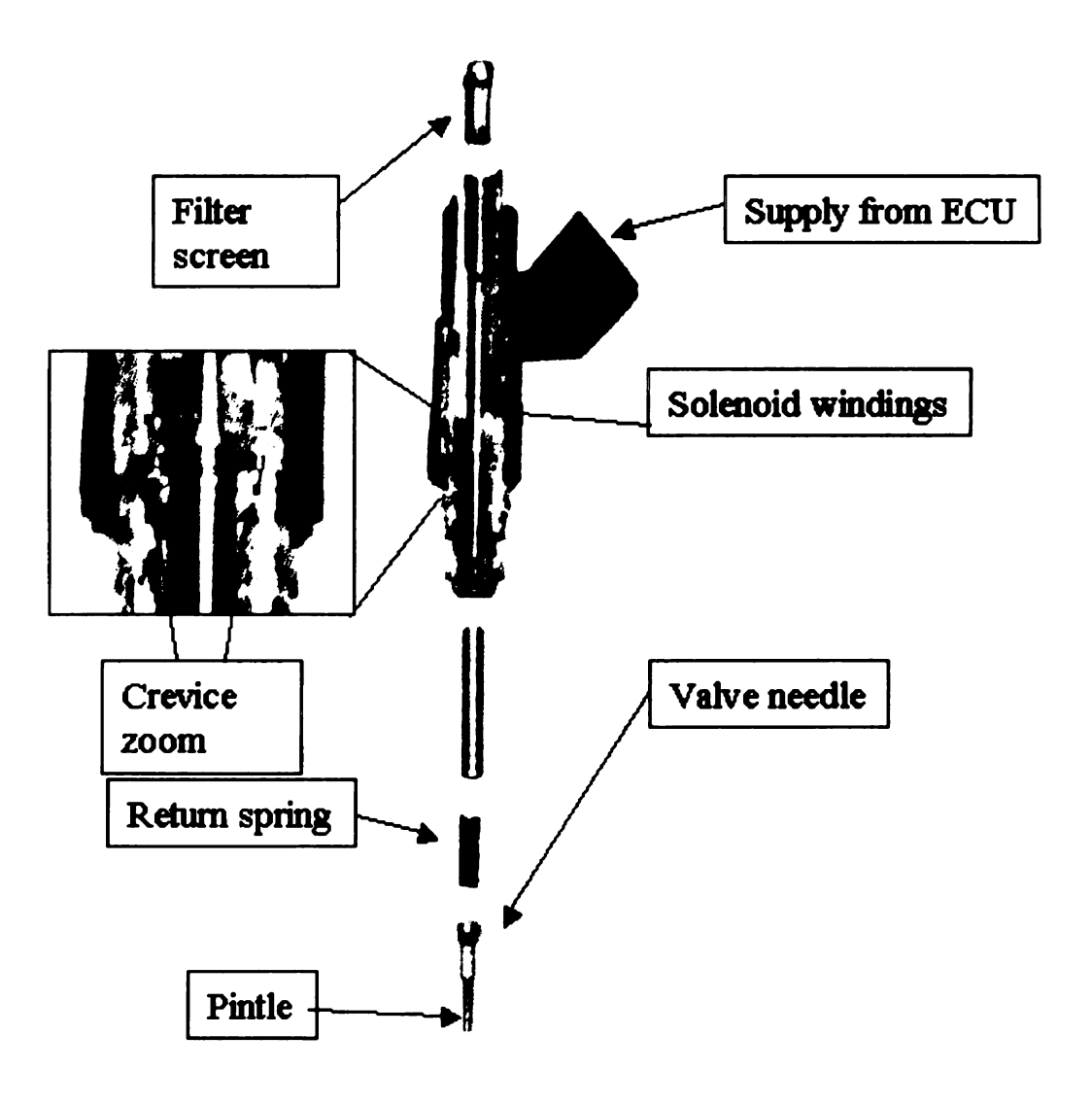


Figure 43: Cutaway of Injector #2. Note crevice zoom.

It would be very interesting to see how the removal of this air influences the variability of the fuel injector. This technique does not allow for that comparison directly. In order to measure the mass injected using centerline velocity measurements, it was assumed that what goes into the injector comes out. If air is present, this is not the case as the bubble is capable of compressing. Thus it is impossible to determine the precise mass injected for comparison with air in the injector using this technique.

In conclusion, air located in the fuel system and/or the injector itself drastically changes centerline velocity. Since most previous studies measure the fuel spray, these bubble dynamics have gone largely unnoticed. Removing the bubbles produces an accurate centerline velocity profile that can then be used as an input to solve more precisely for the mass injected for each injection event.

References

REFERENCES

- [1] Nixon, M., http://www.motorcycleproject.com/motorcycle/text/inject.html.
- [2] Sparks, L., http://chevythunder.com/fuel%20injection%20history.htm.
- [3] Woron, W. "Road Test: 1957 Chevrolet Corvette," Motor Trend, April 2003.
- [4] HowStuffWorks.com educational website, http://auto.howstuffworks.com/fuel-injection.htm.
- [5] Heywood, J. B., *Internal Combustion Engine Fundamentals*, McGraw-Hill Publishing Company, 1988.
- [6] Winterhagen, Johannes, "Siemens VDO Automotive's Piezo Technology Helps Improve Gasoline Engine Fuel Efficiency", Siemens web article, http://www.siemens.com/index.jsp?sdc_rh=null&sdc_flags=null&sdc_sectionid=0 &sdc_secnavid=0&sdc_3dnvlstid=&sdc_countryid=0&sdc_mpid=0&sdc_unitid=9 99&sdc_conttype=2&sdc_contentid=1174392&sdc_langid=1& 2004.
- [7] Stone, R., Introduction to Internal Combustion Engines, SAE International, 2000.
- [8] Ismailov, M. M and Schock, H. J., "Performance Evaluation of a Multi-Burst Rapidly Operating Secondary Actuator applied to Diesel Injection System," SAE Technical Paper 2004-01-0022, 2004.
- [9] Ismailov, M. M. and Schock, H. J., "Quantification of Instantaneous Diesel Flow Rates in Flow Generated By a Stable and Controllable Multiple Injection System (ROSA)," SAE Technical Paper 2004-01-0028, 2004.
- [10] Kainz, J. L. and Smith, J. C., "Individual Cylinder Fuel Control With a Switching Oxygen Sensor," SAE Technical Paper 1999-01-0546, 1999.
- [11] Hung, D. L., Dhmiel, D. M., and Markle, L. E., "Application of an Image-based Diagnostic Technique to Quantify the Fuel Spray Variations in a Direct-Injection Spark-Ignition Engine," SAE Technical Paper 2003-01-0062, 2003.
- [12] Lefebvre, A., Atomization and Sprays, Taylor and Francis, 1989
- [13] Hung, D. L., Humphrey, W. A. et al., "A Novel Transient Drop Sizing Technique for Investigating the Role of Gasoline Injector Sprays in Fuel Mixture Preparation," SAE Technical Paper 2004-01-1349, 2004.

- [14] Brereton, G. B., "The Interdependence of Friction, Pressure Gradient, and Flow Rate in Unsteady Laminar Parallel Flows," *Physics of Fluids*, Vol. 12:3, March 2000.
- [15] Brereton, G.B., Schock, H.J., Rahi, M.A., and Bedford, J.C., "Some Indirect Techniques for Measuring Instantaneous Flow Rates in Unsteady Duct Flows," submitted to *Experiments in Fluids*, 2004.
- [16] Dantec Dynamics Website, http://www.dantecmt.com/LDA/Princip/Index.html.
- [17] Ribbens, W. B., Mansour, N.P. et al., *Understanding Automotive Electronics*, 6th *Edition*, Newnes, 2003

